

AD A 129063

UNCLASSIFIED

SECURITY CLASSIFICATION OF THIS PAGE (When Data Entered)

| REPORT DOCUMENTATION PAGE | | READ INSTRUCTIONS BEFORE COMPLETING FORM |
|--|---|---|
| 1. REPORT NUMBER | 2. GOVT ACCESSION NO. <i>AD A129 663</i> | 3. RECIPIENT'S CATALOG NUMBER |
| 4. TITLE (and Subtitle) Automated Radiography A State-of-the-Art Survey | | 5. TYPE OF REPORT & PERIOD COVERED |
| 7. AUTHOR(s) C. Gerald Gardner | | 6. PERFORMING ORG. REPORT NUMBER NTIAC 78-1 |
| 9. PERFORMING ORGANIZATION NAME AND ADDRESSES NTIAC, Southwest Research Institute P.O. Drawer 28510 San Antonio, TX 78284 | | 8. CONTRACT OR GRANT NUMBER(s) DLA900-77-C-3733 |
| 11. CONTROLLING OFFICE NAME AND ADDRESS Defense Logistics Agency Headquarters Cameron Station Alexandria, VA 22314 | | 10. PROGRAM ELEMENT, PROJECT, TASK AREA & WORK UNIT NUMBERS |
| 14. MONITORING AGENCY NAME & ADDRESS (if different from Controlling Office) Army Materials and Mechanics Research Center Watertown, MA 02172 | | 12. REPORT DATE June 1978 |
| | | 13. NUMBER OF PAGES 36 |
| | | 15. SECURITY CLASS. (of this report) Unclassified |
| | | 15a. DECLASSIFICATION/DOWNGRADING SCHEDULE |
| 16. DISTRIBUTION STATEMENT (of this Report) Approved for public release; distribution unlimited. | | |
| 17. DISTRIBUTION STATEMENT (of the abstract entered in Block 20, if different from Report) | | |
| 18. SUPPLEMENTARY NOTES For Sale by NTIAC, Southwest Research Institute, P.O. Drawer 28510, San Antonio, TX 78284 (\$23.00) | | |
| 19. KEY WORDS (Continue on reverse side if necessary and identify by block number) radiation, gaging, automation, radiography, state-of-the-art reviews, x rays, gamma rays, industrial applications, theory, images, arrays, sources, image quality, optical images, penetrameters, digital systems, analog systems, artillery, filmless techniques, image intensification, display systems, NTIAC | | |
| 20. ABSTRACT (Continue on reverse side if necessary and identify by block number) Radiography employing x-rays and gamma rays is the oldest of the sophisticated methods of nondestructive evaluation. As conventionally practiced, the method involves the use of photographic film or paper, specially prepared for radiography, with the attendant steps of exposure, processing, and finally, visual examination by a skilled 'reader' for indications of flaws in the test piece. While film radiography has certain inherent graphic record of the test, there are many instances where the elimination of film | | |

DD FORM 1473
1 JAN 73

EDITION OF 1 NOV 65 IS OBSOLETE

UNCLASSIFIED

SECURITY CLASSIFICATION OF THIS PAGE (When Data Entered)

UNCLASSIFIED

SECURITY CLASSIFICATION OF THIS PAGE (When Data Entered)

(20) Cont'd.

or human interpretation of the image or both would be highly desirable. This publication surveys briefly the current status of those technologies which are crucial to automated radiography, as well as progress to date in the realization of automated radiography. Two major impediments to fully automated radiography have prevented implementation on an appreciable scale. First, filmless image receptors of sensitivity, resolution, and equivalent image size to radiographic film have yet to emerge. Second, until quite recently, the technical means for automatic image interpretation have not been available. It now appears that both these impediments are likely to be overcome, and that cost-effective fully automated inspection for certain applications, such as artillery shells or components thereof will become a reality in the next few years.

↑

UNCLASSIFIED

SECURITY CLASSIFICATION OF THIS PAGE (When Data Entered)

NTIAC-78-1

AUTOMATED RADIOGRAPHY A STATE-OF-THE-ART SURVEY

by

C. Gerald Gardner
Professor, University of Houston
Formerly Director NTIAC
Southwest Research Institute
San Antonio, Texas

June 1978

NONDESTRUCTIVE TESTING INFORMATION ANALYSIS CENTER

Approved for public release; distribution unlimited

| | |
|--------------------|-------------------------------------|
| Accession For | |
| NTIS GRA&I | <input checked="" type="checkbox"/> |
| DTIC TAB | <input type="checkbox"/> |
| Unannounced | <input type="checkbox"/> |
| Distribution | |
| # 23-01 NTIAC | |
| Distribution/ | |
| Availability Order | |
| Dist | Avail Order |
| A | 21 |



83 05 26 11

TABLE OF CONTENTS

| | <u>Page</u> |
|---|-------------|
| LIST OF ILLUSTRATIONS | iv |
| 1.0 INTRODUCTION | 1 |
| 1.1 Objective | 1 |
| 1.2 Scope | 1 |
| 1.3 Organization of Report | 1 |
| 2.0 PRINCIPLES OF RADIOGRAPHIC IMAGING SYSTEMS | 2 |
| 2.1 The Radiographic Process | 2 |
| 2.2 Characterization of Radiographic Images | 4 |
| 2.2.1 Image Quality Indicators | 4 |
| 2.2.2 Optical Transfer Functions (Ref. 5) | 5 |
| 3.0 COMPUTER PROCESSING AND INTERPRETATION OF IMAGES | 9 |
| 3.1 Digital Images (Ref. 5, 7) | 9 |
| 3.2 Film Image Digitizers | 10 |
| 3.3 Commercial Image Analyzers | 10 |
| 3.3.1 Introduction | 10 |
| 3.3.2 Analog Systems | 10 |
| 3.4 Automated Radiography of Artillery Shells | 12 |
| 3.5 Cavity and Crack Detection | 14 |
| 4.0 FILMLESS IMAGE ACQUISITION SYSTEMS | 19 |
| 4.1 Introduction | 19 |
| 4.2 X-ray Sensitive Image Intensifier Tubes | 19 |
| 4.3 Fluorescent Screen Plus Television | 20 |
| 4.3.1 Fluorescent Screens plus Image Orthicons | 20 |
| 4.3.2 Fluorescent Screen plus Light Intensifier Tubes, plus TV Vidicons | 21 |
| 4.4 X-Ray Sensitive Television Camera Tubes | 21 |
| 4.5 Solid State Radiographic Screens | 24 |
| 4.6 Flying Spot Systems | 26 |
| 5.0 CONCLUSION | 29 |
| REFERENCES | 30 |

LIST OF ILLUSTRATIONS

| <u>Figure</u> | | <u>Page</u> |
|---------------|--|-------------|
| 1 | Basic Radiographic System | 2 |
| 2 | Origin of Geometrical Unsharpness | 3 |
| 3 | Radiography with Multiple Source Array | 3 |
| 4 | Unsharpness Produced by Scatter | 4 |
| 5 | Radiographic Differential Thickness Sensitivity Measured by a Step Wedge | 4 |
| 6 | Typical Radiographic Hole-type Image Quality Indicator (Penetrameter) . | 5 |
| 7 | Significance of Radiographic Resolution | 5 |
| 8 | Basic Imaging System | 6 |
| 9 | Point Spread of Source of Finite Size | 7 |
| 10 | Optical Transfer Function and Modulation Transfer Function for Object Imaged by Source of Finite Size | 8 |
| 11 | Digitized Image as Array of Pixels | 9 |
| 12 | Functional Block Diagram (From Ref. 9, Reproduced by permission of the Society of Photo-Optical Instrumentation Engineers, Palos Verdes Estates, CA) | 11 |
| 13 | Image Enhancer (From Ref. 10, Reproduced by permission of the American Society for Nondestructive Testing, Inc., Columbus, OH) | 12 |
| 14 | Edge Enhancer Block Diagram (From Ref. 10, Reproduced by permission of the American Society for Nondestructive Testing, Inc., Columbus, OH) | 13 |
| 15 | Delineated Segments of the HE Filler (From Ref. 12, Reproduced by permission of Picatinny Arsenal, Dover, NJ, from earlier solicitation document QRI-109) | 14 |
| 16 | Representative Single Scan Across a Pipe Cavitation (From Ref. 12, Reproduced by permission of Picatinny Arsenal, Dover, NJ, from earlier solicitation document QRI-109) | 15 |

| | | |
|----|---|----|
| 17 | Two Representative Pipe Cavity Profiles Used as Templates for Pipe Cavity Detection (From Ref. 12, Reproduced by permission of Picatinny Arsenal, Dover, NJ, from earlier solicitation document QRI-109) | 16 |
| 18 | Cumulative Error Function and Threshold Function for Representative Template (From Ref. 12, Reproduced by permission of Picatinny Arsenal, Dover, NJ, from earlier solicitation document QRI-109) | 17 |
| 19 | Schematic Diagram of a Phillips Type Image Intensifier Tube (From Ref. 4, Reproduced by permission of Butterworths, London, England) | 19 |
| 20 | Schematic Diagram of a Marconi-Fluorex Image Intensifier Tube (From Ref. 4, Reproduced by permission of Butterworths, London, England) | 20 |
| 21 | Modulation Transfer Function for a Fluorescent Screen/Image Orthicon Television System, Calculated from MTF data for the Components (From Ref. 14, Reproduced by permission of Academic Press Inc., London, Ltd.) | 21 |
| 22 | Schematic Diagram of Cinelix Image Intensifier Apparatus (From Ref. 4, Reproduced by permission of Butterworths, London, England) | 22 |
| 23 | Modulation Transfer Function for System Comprising a Fluorescent Screen, Mirrors, Light Amplifier, and System for Film Recording (From Ref. 14, Reproduced by permission of Academic Press Inc., London, Ltd.) | 23 |
| 24 | Diagram of X-Ray Sensitive Vidicon Tube (From Ref. 17, Reproduced by permission of the American Society for Nondestructive Testing, Inc., Columbus, OH) | 23 |
| 25 | Skeletal of X-Ray TV System (From Ref. 17, Reproduced by permission of the American Society for Nondestructive Testing, Inc., Columbus, OH) | 24 |
| 26 | Schematic Diagram of Photoconductive-Electroluminescent Image Amplifier (From Ref. 20, Reproduced by permission of the Society of Photo-Optical Instrumentation Engineers, Palos Verdes Estates, CA) | 25 |
| 27 | Transfer Characteristics of a PC-EL Radiographic Amplifier Screen (From Ref. 20, Reproduced by permission of the Society of Photo-Optical Instrumentation Engineers, Palos Verdes Estates, CA) | 26 |
| 28 | Schematic Diagram of a Flying Spot X-Ray Imaging System for Parcel Inspection (From Ref. 21, Reproduced by permission of the American Society for Nondestructive Testing, Inc., Columbus, OH) | 27 |

29

Schematic Diagram of a Possible Backscattered X-Ray Imaging System
(From Ref. 21, Reproduced by permission of the American Society for
Nondestructive Testing, Inc., Columbus, OH) 28

1.0 INTRODUCTION

1.1 Objective

X-ray and gamma ray radiography is perhaps the most widely employed method of industrial nondestructive evaluation (NDE)*. As conventionally practiced, the method involves the use of photographic film which is exposed, developed, and visually examined by a skilled "reader" for image features indicative of irregularities (flaws) in the radiographed test piece. Film radiography often has many advantages in terms of sensitivity, resolution, and the provision of a permanent graphic record of test results. There are, however, many instances in which it would be desirable to eliminate either the film or the human interpretation of the image, or both. For example, wherever a large number of test articles must be one hundred percent inspected and evaluated, automation of the procedure becomes desirable. Two major technical impediments to the realization of fully automated radiography have prevented its implementation on an appreciable scale. First, filmless image receptors of sensitivity, resolution, and image size equal or superior to film have not emerged, though considerable progress has been made. Second, until quite recently, the technical means of automatic image interpretation have not been available. It now appears that both these impediments can be overcome, and that cost-effective fully automated radiography for at least some important industrial applications will become a reality within the next few years.

It is the objective of this report to survey briefly the current state of the art of those technologies which are crucial to automated radiography, as well as progress to date in realizing automated radiography.

1.2 Scope

This report is based on a review of pertinent open technical literature. Thus, current work in progress, but not yet openly reported, is not covered here. The literature retrieval was accomplished by the Nondestructive Testing Information Analysis Center by searching pertinent computerized documentation data bases, the most recent search having been concluded in December, 1976.

The scope of this report is limited to developments that relate to conventional two-dimensional grey-scale images, of which the conventional film radiograph is the archetype. Thus, systems which involve only radiometry (radiation gauging) in a manner which does not lead to a two-dimensional image (or its equivalent) are not considered. Likewise, systems which lead to a three-dimensional (tomographic) representation of a test article are not included. Although much of the discussion here is applicable to radiography with sources other than x-rays or gamma rays, (e.g., neutrons), such types of radiography are not expressly considered. No value judgment is intended by these restrictions.

It is assumed that the reader is generally familiar with conventional film radiography. A brief review of some essential concepts is presented in Section 2. Suitable background material may be found in References 2, 3, 4, and other references cited therein.

1.3 Organization of Report

In Section 2 the principles of the radiographic process, the characterization of images, and the characterization of imaging systems are reviewed. In Section 3 the automatic processing and interpretation of film images is discussed. Various approaches to filmless image acquisition are presented in Section 4. Finally, in Section 5 some general conclusions are drawn.

*The term "nondestructive evaluation," rather than "nondestructive testing" or "nondestructive inspection," has been recommended by the National Materials Advisory Board (Ref. 1).

2.0 PRINCIPLES OF RADIOGRAPHIC IMAGING SYSTEMS

2.1 The Radiographic Process

The following brief discussion is limited to those aspects of the radiographic process which are essential to the ensuing discussion of automated radiography. For a more comprehensive treatment, References 2, 3, and 4 may be consulted.

In its simplest form a radiographic system comprises a "point" source of radiation, the object to be radiographed, and an "image receptor" on which a "shadow" of the test object is projected (Figure 1). The

radiation penetrates the test object, is attenuated by it, and falls on the image receptor (e.g., photographic film). In the absence of the test object, the intensity of radiation, measured along a ray emanating from the source, falls off as the reciprocal of the square of the distance from the source. As a ray passes through the test object, the intensity of the radiation is attenuated by absorption and by scattering. The net attenuation along a given ray is determined by the physical properties of the matter composing the test object, and the total path length through the material. A discontinuity (void, inclusion, etc.) is, in effect, a change in the path length traversed by a ray passing through the discontinuity. Thus, there is formed a two-dimensional pattern of radiation intensity, which may be represented by a function $I(x, y)$ where x and y are coordinates in the image plane. The response of the image receptor (e.g., the optical density of a photographic film after development) at a point (x, y) in the image plane is, in general, a monotonically increasing function of the total exposure $E(x, y)$, i.e., the product of $I(x, y)$ and the exposure time t . The characteristic of the image receptor of prime importance is not its absolute response, R , to a given exposure; but the difference in response to slightly different exposures, i.e., dR/dE . At the image receptor, two regions of slightly different response are said to have a contrast, C , equal to $\Delta R/R$, where ΔR is the difference in response and R is the mean response. Thus, in the case where photographic film is the image receptor, if the optical density, $D(x, y)$, of the exposed and developed film were completely uniform (or completely random), the "image" would contain no useful information.

Referring to Figure 1, the projected image-plane dimension L_i is related to the corresponding object feature of (lateral) dimension L_o by the equation:

$$\frac{L_i}{L_o} = \frac{d_{si}}{d_{so}}$$

where d_{so} and d_{si} are respectively the source-to-object distance and the source-to-image plane distance. The geometrical magnification, M , is thus d_{si}/d_{so} .

In practice the radiation source is of finite effective aperture; this results in "geometrical unsharpness" of the image, as illustrated in Figure 2. Geometrical unsharpness is minimized when the object-to-image plane distance is minimal. Thus, the image produced by a ray, ideally a point, is "smeared" into a continuous distribution. (Some proposed radiographic systems would employ multiple sources in an array, with collimators employed to achieve a beam of large cross-section, with approximate parallel rays, as illustrated in

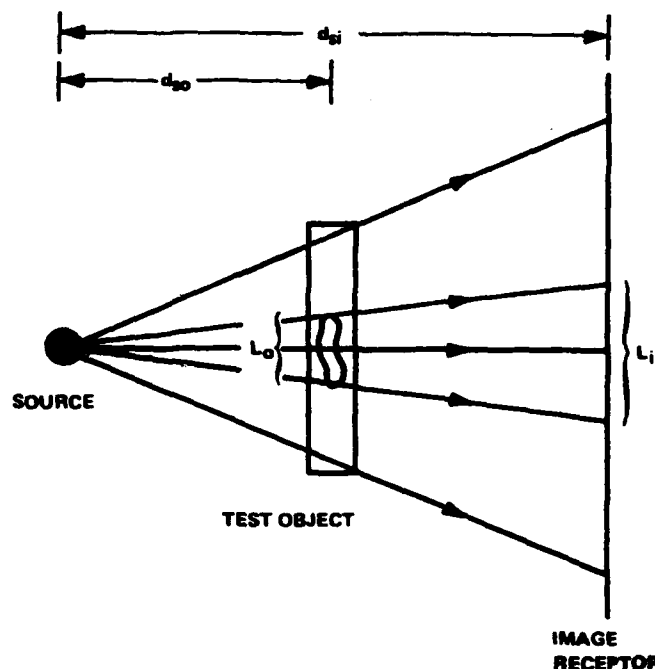


Figure 1. Basic Radiographic System

Figure 3. The image produced by such a system is made up of an array of small images, each produced primarily by a corresponding single source. Geometrical enlargement of the image is thus small, and beam intensity, measured along a ray, is approximately constant. The image is, however, subject to geometrical unsharpness determined by source aperture, d_{so} and d_{si} , in the same manner as for a single-source arrangement.)

As a ray of radiation passes through an object, some of the radiation is scattered, as illustrated in Figure 4. When radiation of a given energy is scattered from the primary ray, the energy of the scattered radiation is reduced. The distribution of scattered radiation, with respect to the direction of a primary incident ray, depends upon the energy (or energy spectrum) of the primary ray, the thickness of the object through which the primary ray has passed, and the material of which the object is made. Thus, the effect of scattered radiation is to reduce both image contrast and sharpness. Various measures may be taken to reduce the adverse effects of scattered radiation; these include the use of thin filter plates between the object and the image plane (which function by preferentially absorbing the lower-energy scattered radiation); the use of collimation grids the openings in which are aligned to pass the primary rays, but intercept the scattered rays; and the use of radiation detectors which are energy selective, with their response peaked at the energy of the primary radiation. (This latter method is most effective when the primary radiation consists of one or more discrete energy components, as is the case with gamma rays emitted by radionuclides).

Another property of radiation affecting the image is that radiation consists of photons, i.e., discrete packets of each photon bearing energy hf , where h is Planck's constant and f is the frequency of the radiation. When a photon is absorbed by an atom or electron, that photon disappears, its energy being acquired by the absorbing atom or electron; scattering actually consists of absorption of a primary photon, followed by emission of a secondary photon. The number of photons in a beam of radiation, of a given average intensity, fluctuate statistically about a mean value. Thus, the number of photons which impinge on a unit area of the image plane, in a given time, differ from point to point in the image plane even when the mean exposure of all points is nominally the same. If the mean number of photons per second per unit area is N , the standard deviation is \sqrt{N} ; the standard deviation divided by the mean is thus, $1/\sqrt{N}$. When N is large, the effect of statistical fluctuation is thus negligible, but when N is small (as it might be when minimal exposure times are needed for rapid inspection), the effects of statistical fluctuation become large. The consequent uncertainty in intensity at a given point in the image plane may thus become the limiting factor in the imaging system. When photographic film is used as an image receptor, the statistical character of photon beams results in statistical fluctuations in optical density; at the lower limit of useful exposure, the film exhibits "quantum mottle" due to the combined effects of fluctuations in the number of photons absorbed and the fact that the photographic image actually consists of individual microscopic "grains" of free silver, each of which may be produced by as few as one photon. Filmless image

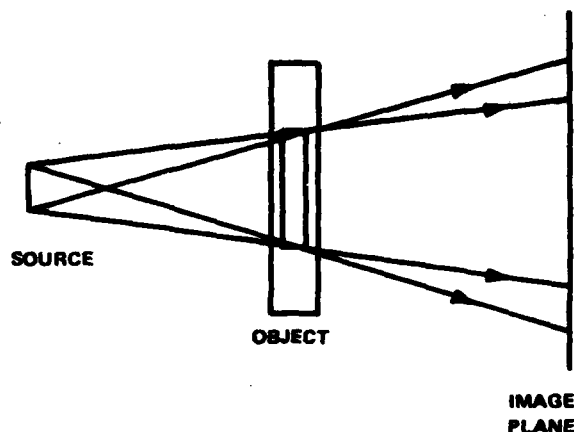


Figure 2. Origin of Geometrical Unsharpness

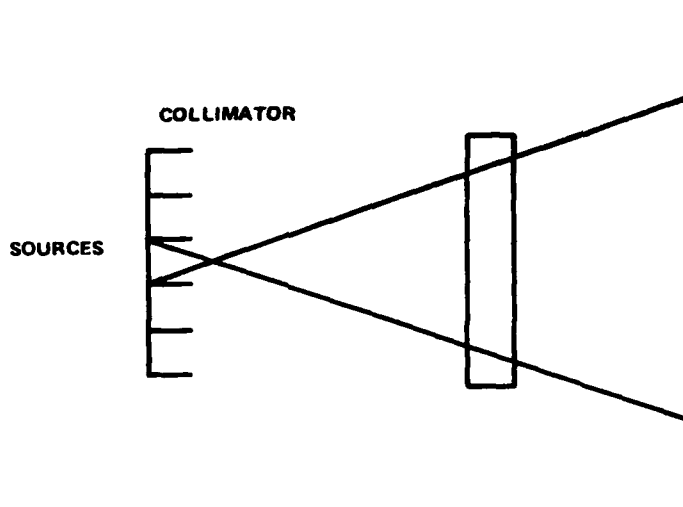


Figure 3. Radiography with Multiple Source Array

receptors are similarly affected by the statistical character of photon beams, although other effects such as intrinsic electronic noise may outweigh the noise due to fluctuations in the arrival rate of photons.

2.2 Characterization of Radiographic Images

2.2.1 Image Quality Indicators

In general, a radiographic image may be thought of as a two-dimensional function $R(x, y)$, x and y being coordinates in the image plane, and R being some response variable; in the case of photographic film, R is the optical density of the film; in the case of a photon counter located at (x, y) , R is the number of counts accumulated during a fixed exposure time. Both information and noise are contained in the image in the form of variations of $R(x, y)$ from point to point in the image plane. For the moment we disregard the question of noise. There are two conventional terms used to characterize radiographic imaging systems, namely *sensitivity* and *resolution*. There is no universally accepted definition of these terms. In general, *sensitivity* refers to the ability of the imaging system to distinguish a region of a test object having an effective equivalent thickness slightly different from the nominal thickness. Sensitivity is therefore primarily related to image contrast. A conventional, practical way of assigning a value to differential thickness sensitivity is by means of a calibrated step wedge, as illustrated in Figure 5. The wedge is made from the same material as the test object (or a "radiographically equivalent" material). The increments in thickness of the wedge are selected to correspond to, say, 1 percent of the thickness of the test object. In conventional film radiography the film reader examines the radiograph and makes a subjective judgment of the minimum thickness of the wedge which he can "reliably" discern visually. He then speaks of "one percent sensitivity," "two percent sensitivity", and so on.

If the flaws to be detected are small in lateral extent, a hole-type image quality indicator ("penetrameter") may be used, as illustrated in Figure 6. A series of holes of varying diameter are drilled in a small plate, the thickness of which is some fraction (say, 2 percent) of the test object. The diameter of the holes is usually a multiple of the thickness, T , of the penetrameter, say $1T$, $2T$, $3T$, etc. The penetrameter is placed on the test object during exposure of the radiograph. The reader then examines the developed radiograph and makes a subjective judgment of the smallest hole he can reliably discern visually. He then speaks of working at $1-1T$, $1-2T$, $2-1T$, $2-2T$ (percent thickness, hole diameter), etc., sensitivity.

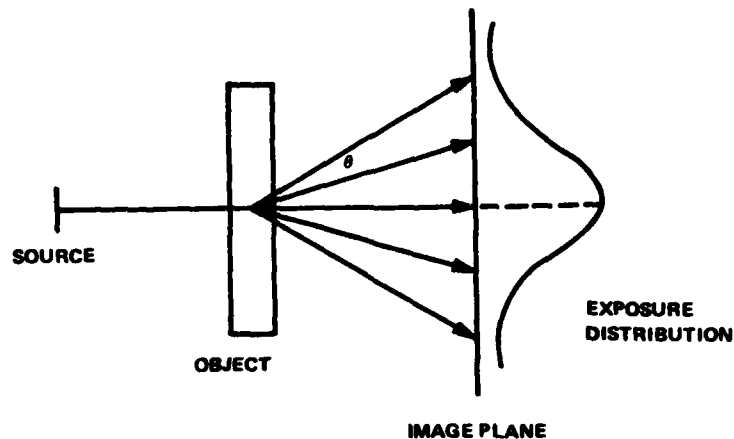


Figure 4. Unsharpness Produced by Scatter.

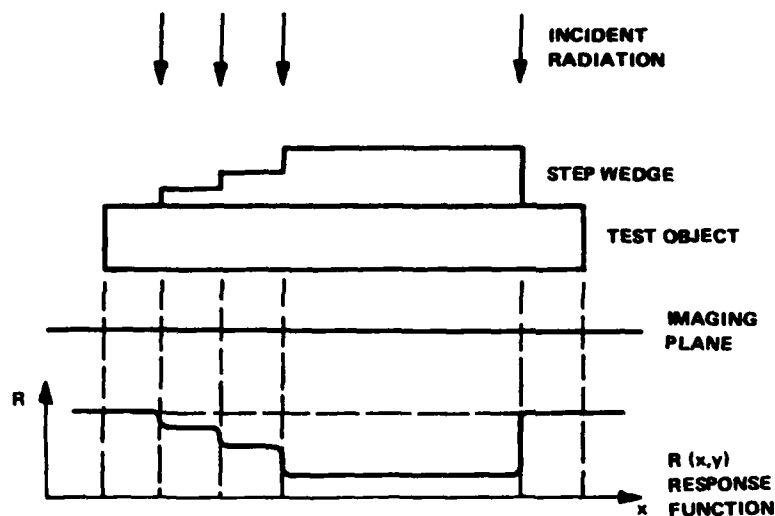


Figure 5. Radiographic Differential Thickness Sensitivity Measured by a Step Wedge

The term *resolution* refers to the ability of a radiographic system to discriminate between two neighboring features which, if well separated, would produce the same contrast in the image receptor. The principle is illustrated in Figure 7. As the two flaws come closer together, it becomes more difficult to discern their images as being separate. Resolution is often expressed as the maximum number of lines per millimeter (or per inch) which can be discerned.

The foregoing methods have the disadvantage of being at best semiquantitative and, in fact, both sensitivity and resolution are "mixed" in their use. For more quantitative and precise characterization, so-called optical transfer functions are coming into use.

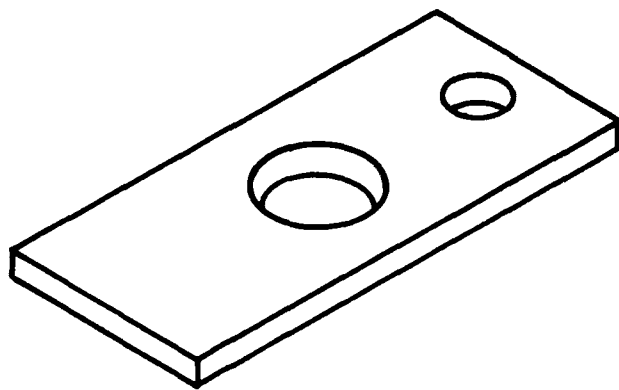


Figure 6. Typical Radiographic Hole-type Image Quality Indicator (Penetrameter)

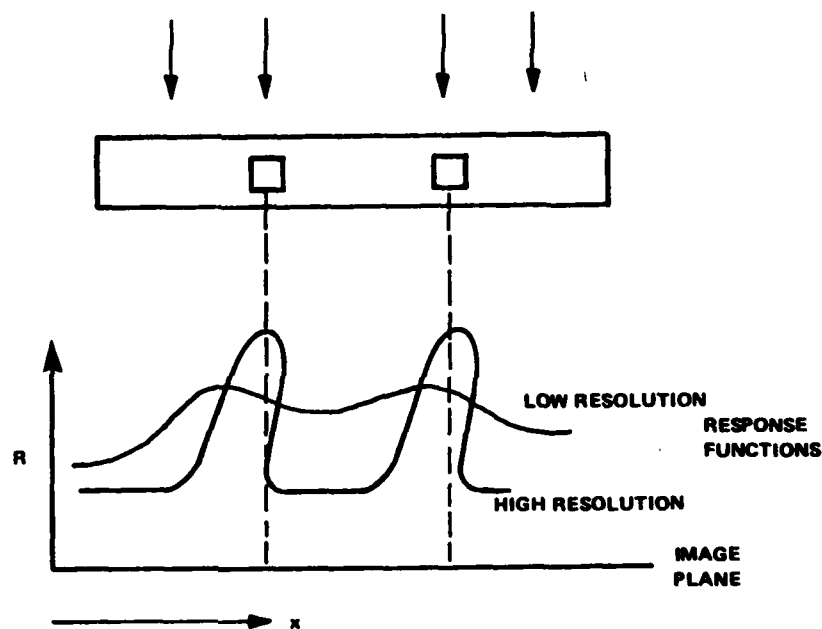


Figure 7. Significance of Radiographic Resolution

2.2.2 Optical Transfer Functions (Ref. 5)

An imaging system may be regarded as a device which maps (transfers) an object plane onto an image plane. The object may be thought of as a two-dimensional distribution of source intensity $S(x', y')$; the image is a corresponding distribution $R(x, y)$, as illustrated in Figure 8. A point (x', y') in the object plane, of unit intensity, is imaged on the image plane as an intensity distribution $p(x', y'; x, y)$. $p(x', y'; x, y)$ is called the point-spread function or impulse response function.

Assuming the image-forming process to be linear, the total image may be expressed by the relation

$$R(x, y) = \int S(x', y') p(x', y'; x, y) dx' dy' \quad \text{Eq(2.2.2-1)}$$

where the integral is over the entire object plane. If the point spread function is the same for all source points, regardless of position (only approximately true for the radiographic process), the point spread function must

be of the form $p(x-y', y-y')$, hence

$$R(x, y) = \int S(x', y') p(x-x', y-y') dx' dy'$$

Thus, $R(x, y)$ is the convolution of S with p .

$R(x, y)$ may be expressed in terms of a two-dimensional Fourier integral:

$$R(x, y) = \int G_R(f_x, f_y) e^{-i2\pi(f_x x + f_y y)} df_x df_y$$

$G_R(f_x, f_y)$ is in turn the Fourier transform of $R(x, y)$:

$$G_R(f_x, f_y) = \int R(x, y) e^{+i2\pi(f_x x + f_y y)} dx dy$$

The transform variables f_x and f_y are spatial frequencies, i.e., cycles per unit length. The total image is thus a superposition of sinusoidally varying components (in the x -direction and y -direction, respectively). The object distribution may be similarly Fourier transformed yielding $G_S(f_x, f_y)$. The point spread function $p(x-x'; y-y')$ may be Fourier transformed yielding $H(f_x, f_y)$. The advantage of the Fourier decomposition lies in the fact that, as a consequence of Equation (2.2.2-1), the object and image transforms are simply related by the equation

$$G_R(f_x, f_y) = H(f_x, f_y) \cdot G_S(f_x, f_y) \quad \text{Eq(2.2.2-2)}$$

In other words, each Fourier component of the object distribution is reproduced in the image distribution, but multiplied by the "transfer function" $H(f_x, f_y)$. It is convenient to work in terms of normalized quantities:

$$g_S(f_x, f_y) = \frac{G_S(f_x, f_y)}{\int S(x', y') dx' dy'}$$

$$g_R(f_x, f_y) = \frac{G_R(f_x, f_y)}{\int R(x, y) dx dy}$$

$$h(f_x, f_y) = \frac{H(f_x, f_y)}{\int p(\xi, \eta) d\xi d\eta}$$

Corresponding to Equation 2.2.2-2 we have

$$g_R(f_x, f_y) = h(f_x, f_y) g_S(f_x, f_y).$$

The normalized transfer function $h(f_x, f_y)$ is called the optical transfer function (OTF). In general the OTF is a complex function; in the case where the point spread function $p(x-x'; y-y')$ is symmetric, i.e., $p(x-x'; y-y') = p(x'-x, y'-y)$, the OTF is a real function. The latter case obtains, at least approximately, in radiographic systems. Even so, the OTF may assume both positive and negative values, with important consequences for radiographic resolution.

The absolute value of the OTF, $|h(f_x, f_y)|$, is called the modulation transfer function (MTF). The MTF has the property $h(f_x, f_y) \leq h(0, 0) = 1$.

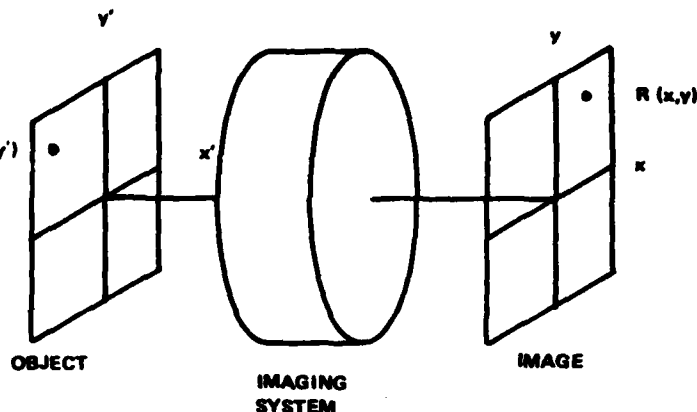


Figure 8. Basic Imaging System

An optical transfer function may be defined for each stage in the image forming process. Assuming overall linearity, the optical transfer function for all stages combined is simply the product of the OTF's for each stage separately; an analogous statement holds for the overall MTF. Thus an OTF may be associated with the geometrical imaging of an x-ray source of finite aperture (geometrical unsharpness), the unsharpness introduced by scattering in a target object of finite thickness, and "point spreading" introduced by the intrinsic properties of the image receptor.

Line Spread Function — If the source distribution $S(x', y')$ is invariant in one direction, say, the y' -direction, so that $S(x', y') = S(x')$, Equation (2.2.2-1) becomes

$$R(x, y) = R(x) = \int S(x') \{ \int p(x', y') dy' \} dx'$$

The function $\mathcal{L}(x') = \int p(x', y') dy'$ is called the line spread function. It represents the response of the imaging system to a line source function of infinitesimal width and unit intensity. The Fourier transform of the line spread function is the optical transfer function for a source distribution with intensity varying only in one direction, for example, the x' -direction; the absolute value of this OTF is the MTF for such a source. The line OTF and MTF for a radiographic system may be determined by radiographing a thin one-step wedge in contact with the test object. The normalized response function $\bar{R}(x)$ is then determined (in the case of film), by means of a scanning densitometer. The Fourier transform of the normalized response function may then be computed numerically; the MTF is the absolute value of the OTF.

The MTF falls off (though not always monotonically) with increasing spatial frequency. Below some value of the MTF, it is no longer possible to discern higher frequency variations in $R(x)$. This upper limit on resolvable spatial frequency (and corresponding lower limit on MTF) is, of course, dependent upon the criterion of "discernibility" that is applied. Whatever the criterion, the upper limit on f may be expressed by stating its reciprocal, $1/f$, which is in cycles per unit length, or, more commonly, lines per unit length. Thus a simple statement of the resolution of a radiographic system in lines resolvable per unit length may be a quite insufficient characterization of the resolution.

That the MTF alone may be an inadequate description of the resolving power of a radiographic system has been emphasized by Gray et al. (Ref. 6) who discuss the OTF of an x-ray source of finite aperture. Referring to Figure 9, and considering only geometrical effects, the point spread function of the source is a square of side $w = ad_2/d_1$. The OTF is the Fourier transform of this figure:

$$OTF(f_x, f_y) = [OTF(f_x)] \cdot [OTF(f_y)] = \frac{\sin(\pi f_x a d_2 / d_1)}{\pi f_x a d_2 / d_1} \cdot \frac{\sin(\pi f_y a d_2 / d_1)}{\pi f_y a d_2 / d_1}$$

The length of an object feature, L_o , is related to the length of its projected image, L_i , by the equation

$$L_i = \frac{d_1 + d_2}{d_2} L_o$$

Thus the spatial frequency referred to the object, f_o , may be related to the spatial frequency referred to the image, f_i , by the equation

$$f_i = \left(\frac{d_2}{d_1 + d_2} \right) f_o$$

Hence the OTF (for either f_x or f_y) may be expressed as

$$OTF(f_o) = \left(\frac{\sin \pi f_o a d_2}{d_1 + d_2} \right) / \pi f_o a d_2 / (d_1 + d_2)$$

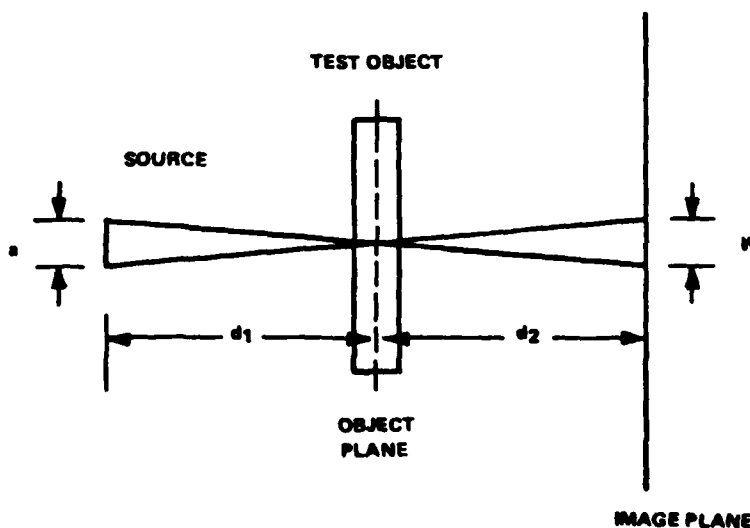


Figure 9. Point Spread of Source of Finite Size

Figure 10 shows a graph of this (one-dimensional) OTF and the corresponding MTF for one choice of a , d_1 , and d_2 . It is to be noted that for frequencies in the interval

$$\frac{d_1 + d_2}{ad_2} < f_0 < \frac{2(d_1 + d_2)}{ad_2}$$

the OTF is negative, signifying that for spatial frequencies in this range there is a reversal of image contrast with respect to object radiographic thickness—regions thicker than the mean are imaged more brightly than the mean (i.e., for film, the density would be greater than the mean), and vice versa! The effect is more than theoretical; Gray et al. (Ref. 6) show a group of five parallel bars so selected in width and separation as to produce a reversal in contrast, thus creating the illusion that there are only four objects radiographed (i.e., the spaces between the five bars). The MTF, being positive at all frequencies, fails to reflect this potential for contrast reversal at certain spatial frequencies. Thus care must be exercised when an MTF curve alone is interpreted in terms of resolution.

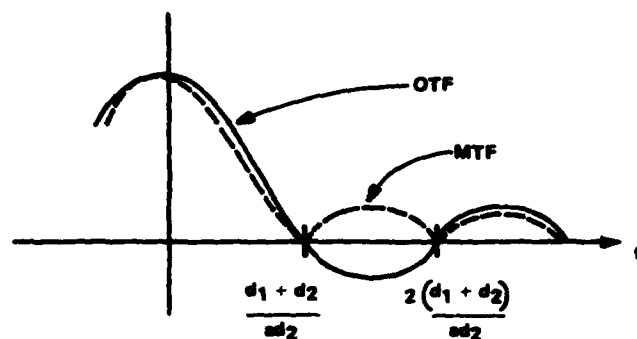


Figure 10. Optical Transfer Function and Modulation Transfer Function for Object Imaged by Source of Finite Size

3.0 COMPUTER PROCESSING AND INTERPRETATION OF IMAGES

3.1 Digital Images (Refs. 5, 7)

A uniformly sampled digital image comprises an $N \times M$ array of pixels (picture elements), each of which is a binary number representing a grey-scale image intensity associated with the coordinates $x = N(\Delta x)$, $y = M(\Delta y)$ in the image plane, the pixel having area $(\delta x)(\delta y)$; (usually $\delta x = \delta y$). (See Figure 11). The extent to which a digital image faithfully captures the information content of the analog intensity distribution to which it corresponds depends upon: (1) the sampling interval Δx , Δy ; (2) the sampling aperture δx , δy ; and the precision of analog-to-digital conversion. The effect of these factors depends primarily upon the spatial frequency content of the original analog image. If the original analog image is band-limited i.e., if the Fourier transform $G_R(f_x, f_y)$ vanishes except for $f_0 \leq f_x$, $f_y \leq f_0 + \Delta f$, (and if degradation produced by other factors is neglected), then it can be shown (Whittaker-Shannon sampling theorem) that the maximum sampling interval permitting faithful recovery of the original analog image is $\Delta x, \Delta y = (2\Delta f)^{-1}$. Thus if the maximum spatial frequency of significant amplitude present in the analog image is 10 lines/mm, the minimum sampling interval for theoretically faithful reproduction is 0.05 mm.

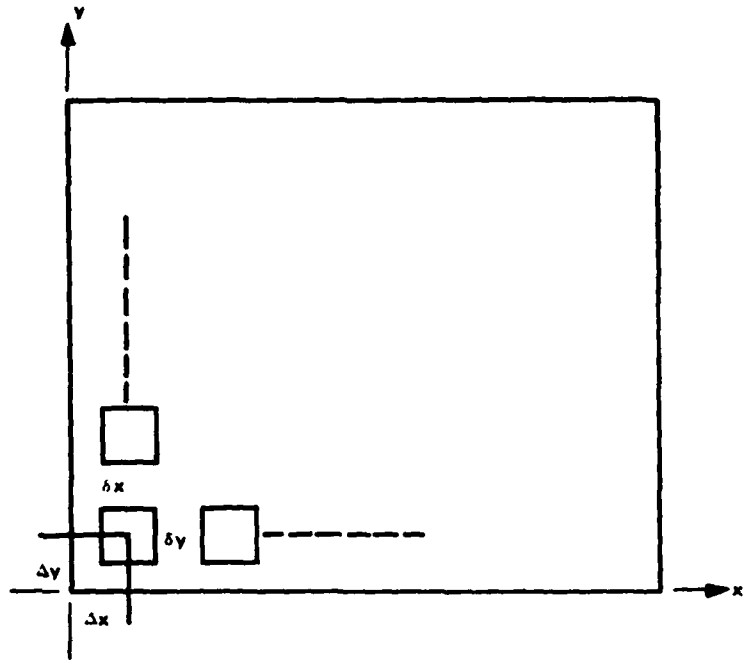


Figure 11. Digitized Image as Array of Pixels

Many computer algorithms have been devised for "processing" a digital image to "enhance" or "restore" it. Still other algorithms have been devised to "recognize" and "extract" certain features which may be present in the image. Algorithms also exist for determining certain characteristics of a recognized feature, e.g., its perimeter, area, maximum (or minimum) linear dimension, etc. Several manufacturers offer sophisticated image analysis systems in which some set of such algorithms is implemented. Usually the commercial systems are especially adapted for specific applications, e.g., biological cells, small particles, etc. Some of these systems are, at least in principle, applicable to radiographic image analysis; however, there have thus far been published no systematic studies of such applications.

Considerable work has been published on studies of applications of computerized analysis of medical radiographic images, and much of this work has a bearing on potential analysis of industrial radiographs. As a rule, however, the software (computer programs) thus far developed has been rather specific to a particular type of image, and has not been generalized to make it readily applicable to general industrial radiographs. Other obstacles to industrial applications are the time required to digitize a radiograph of dimensions typical in industry, as well as the fact that rather large computers (especially in terms of core or other rapid access memory) are required, and computational times for analyzing a large image are discouragingly long. However, this field is progressing rapidly on both the software and hardware fronts, and it seems probable that the major obstacles will be overcome within the next few years. (Work is currently in progress to adapt and develop computerized digital image analysis to radiographs of artillery shells, [Lockheed Palo Alto Research Laboratory, Contract DAAA21-76-CO512 with ARRADCOM]). Technical details are unavailable at this writing.

In the ensuing sections, the general state of digital image enhancement and feature recognition, as particularly related to NDE, is reviewed. Finally, one specific attempt to achieve automatic interpretation of

radiographs of 105 mm high-explosive shells is reviewed; this latter attempt appears to be the only one expressly related to NDE, the details of which have been published in the open technical literature.

3.2 Film Image Digitizers

If film is used as an intermediary in an automated radiographic system, the system must include a means of converting the film grey-scale image to either analog electronic form or digital form. Perhaps the simplest way of doing this is to use essentially the standard type of light box to illuminate the developed radiograph, and replace the human viewer with a television camera. The resultant video signal is the scan raster equivalent of the radiographic image. With appropriate logarithmic amplification of the video signal, the image displayed on a television monitor will have brightness inversely proportional to the corresponding film density. An example of such a film-to-video converter is discussed in Paragraph 3.3.2.

Although the video signal from a television camera viewing a radiograph could be sampled and digitized, more direct means are necessary for high spatial resolution and A-to-D conversion accuracy. Scanning densitometers provide this.

The greatest accuracy and resolution is achieved with a fixed densitometer and a mechanically moveable x-y coordinate bed, the x- and y- coordinates being controlled by precision machine screws driven by stepper motors which are in turn computer controlled. Hunt et al. (Ref. 8) describe such a system. Their x-y bed accommodated radiographs up to 14 in. by 17 in. Square scanning apertures in the range from 10 microns to 200 microns are used. The minimum sampling interval (both x and y) was 10 microns. Allowable film density range for apertures up to 50 microns was 0.0 to 3.0; for apertures greater than 50 microns, the range was 0.0 to 5.0. Each density value was coded as a 9-bit (8-bit resolution, i.e., 1 part in 256) binary number written on magnetic tape. Approximately one hour was required to digitize a 13 in. by 13 in. area with a 100-micron raster spacing in both x and y. An image may be "played back" on the same system. Play-back was limited to 6 bits (64 grey-scale levels). A maximum play-back density of 2.0 is achievable with film of speed equivalent to Kodak Tri-X. The scanner/playback system was controlled by a minicomputer with 8,000 12-bit words of core memory.

In addition to the flat x-y bed scanning densitometer, drum-type scanning densitometers are also commercially available.

To achieve substantially shorter image digitization times, mechanical scanning schemes must be abandoned. A system which employs a moving light spot on the face of a cathode ray tube has been described by Ett and Merritt (Ref. 9). A functional block diagram of the system is shown in Figure 12. Spot sizes down to 0.7 mils diameter were possible. The CRT beam location was precisely controlled; spot location addressing resolution was 12 bits (4096 points per line); drift was less than 0.02%. Grey-level encoding was 6 bits (64 levels). This system was basically designed to handle 70-mm photographic film, but it is said that with appropriate optics essentially any film size can be accommodated. The same system may be used "in reverse" for image read-out. Representative image digitization rates were not cited, but one image of unspecified dimensions was reported to have been digitized in 3 seconds. Effective optical modulation transfer functions or an equivalent resolution figure were not stated.

3.3 Commercial Image Analyzers

3.3.1 Introduction

A number of image analyzer systems are currently commercially available. They are of two general types, analog and digital. Both types are essentially video systems which require "hard copy" input (i.e., film in the case of radiography). Such systems are not expressly adapted for radiographic applications, nor are they fully automatic except for certain types of simple images. Such systems (or derivatives from such systems) may in due course be integrated into fully automated radiographic systems, and will therefore be briefly described.

3.3.2 Analog Systems

Vary has described efforts to apply a representative electronic image analyzer to radiographs (Ref. 10). The system he used is illustrated in Figure 13; a block diagram of the system is shown in Figure 14.

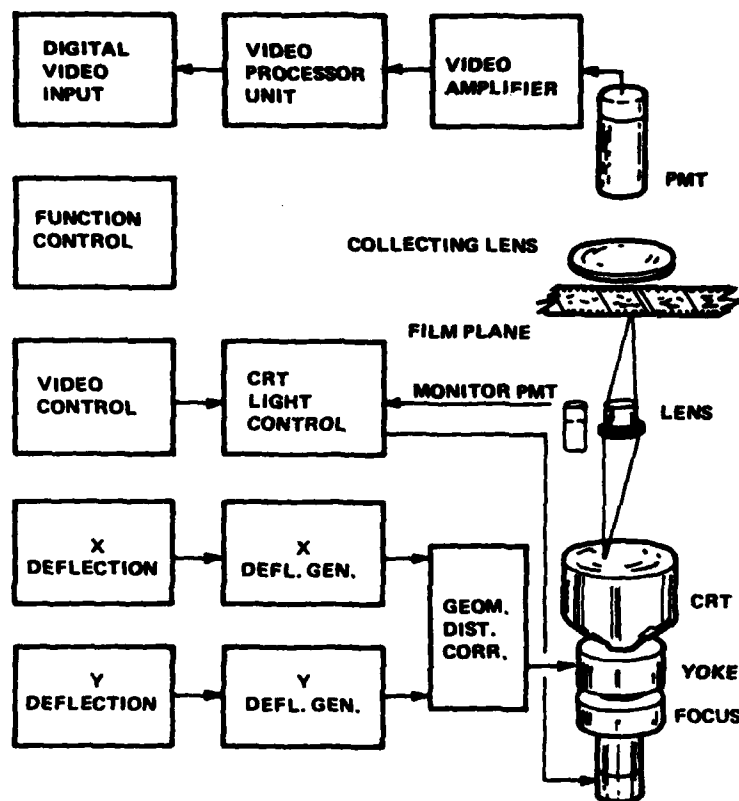


Figure 12. Functional Block Diagram (From Ref. 9, Reproduced by permission of the Society of Photo-Optical Instrumentation Engineers, Palos Verdes Estates, CA)

This system employs a vidicon camera to view a radiograph on an illuminator, through one of several optional lenses giving optical magnification up to 30X. The camera used had a standard 525 line raster, with a measured resolution of approximately 600 vertical lines and 500 horizontal lines; the dynamic range was 2.4 density units (roughly corresponding to that of typical film radiographs). The "unprocessed" image could be displayed on a (black and white) television monitor, or it may be processed through a logarithmic amplifier to produce an image with brightness proportional to film density (electronic contrast reversal is possible). Edge enhancement is obtained by delaying the density signal and subtracting it from itself (roughly a differentiation of the signal). The greater the rate of change of density at edges, the greater the brightness of the enhanced edges; substantial edge broadening occurs in this process. The edge enhancer responds, of course, only to edges which are not parallel to the raster scan lines.

Vary reports that the enhancer resolves better than 60 line-pairs per millimeter at an optical magnification of 30X; a half-mil diameter wire was resolved at a magnification between 10x and 20x, against a background in which it was barely visible without enhancement. Vary observes, however, that with "some exceptions" the enhanced video displays reveal nothing that could not be discerned by direct eye viewing of the original radiographs (with proper visual technique).

Vary and Bowles also studied a more elaborate version of the foregoing system, providing video densitometry, video micrometry, and density slicing (Ref. 11). The system provides a pseudocolor display in which up to four colors are made to correspond to isodensity patterns, within any selected portion of the optical density range present in the radiograph. A "density sliced" image may be obtained by suppressing all

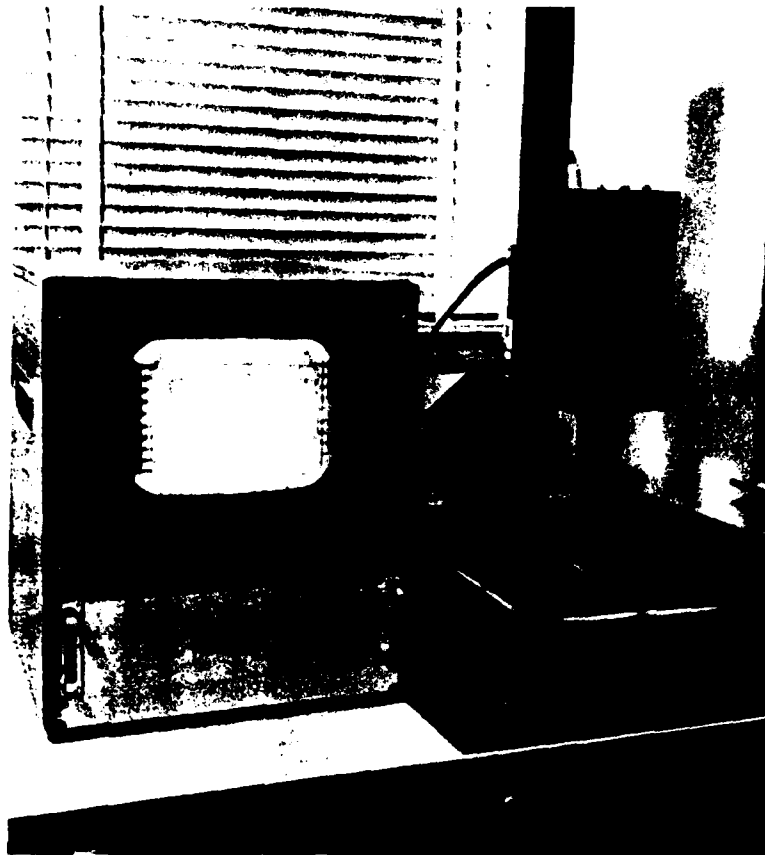


Figure 13. Image Enhancer (From Ref. 10, Reproduced by permission of the American Society for Nondestructive Testing, Inc., Columbus, OH)

colors save one. Provision is also made for superimposing upon the normal video image display a tracer corresponding to the radiographic density profile along a selected raster line. Provision is also made for two electronically generated cursors (marker lines) which are superimposed on the displayed image, and with appropriate controls can be manually aligned with image features of interest; separation between the cursors is displayed on a digital meter (which must be appropriately calibrated).

3.4 Automated Radiography of Artillery Shells

The University of California, Los Alamos Scientific Laboratory studied a computer-based system for automatically interpreting conventional film radiographs of 105-mm high-explosive shells (Ref. 12). The development was sponsored by the Picatinny Arsenal of the U.S. Army. (This project aimed at ultimate elimination of film as a recording and storage medium). The development was concerned with flaws in the melt-poured high-explosive filler. Defects of concern include cracks, cavities, porosity, and separation of the filler from the shell at the base. For purposes of analysis, the HE filler is divided into four segments, A, B, C, and D, as illustrated in Figure 15. The maximum permissible defect is generally larger as one proceeds from A to D. These maxima are bounded by 0-1.9 cm for linear measures, and by 3.25 cm² for projected area measured.

The analysis was divided into four sequential phases:

- (1) Detection of shell macrostructure for the purpose of scene segmentation.
- (2) Detection of regions within the segmented shell scene containing cavitations.
- (3) Measurement of detected anomalies.

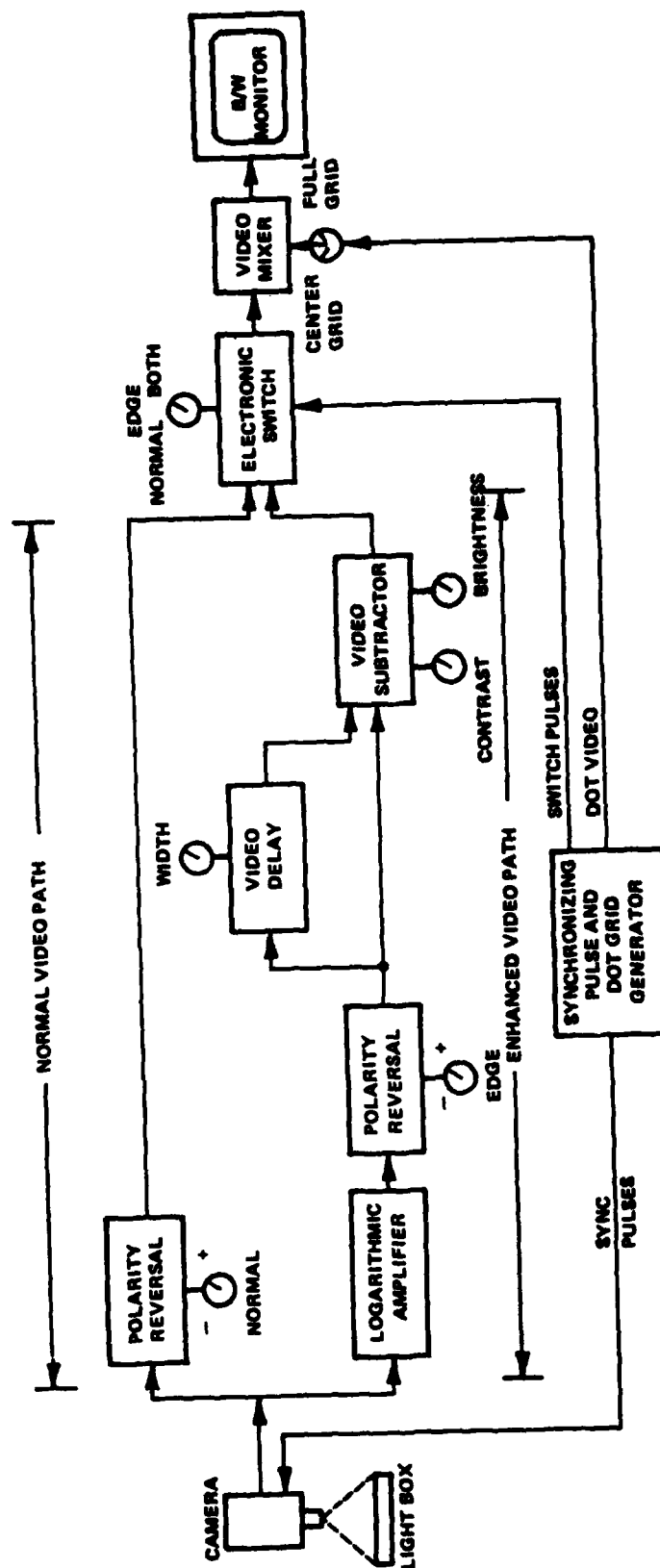


Figure 14. Edge Enhancer Block Diagram (From Ref. 10, Reproduced by permission of the American Society for Nondestructive Testing, Inc., Columbus, OH)

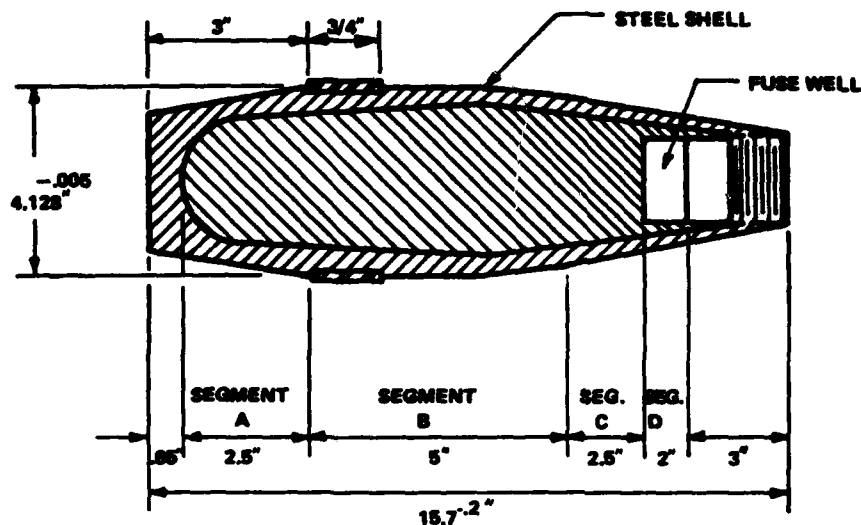


Figure 15. Delineated Segments of the HE Filler (From Ref. 12, Reproduced by permission of Picatinny Arsenal, Dover, NJ, from earlier solicitation document QRI-109)

- (4) Classification of shells into an accept or reject category. Initial work on the first two phases has been reported to date.

Typically four shells are radiographed at once, their image appearing side by side on the same sheet of film. The image is digitized by means of a scanning densitometer. Each projectile is represented by a digital matrix with 444 rows and 128 columns (56, 832 picture elements).

A computer algorithm was developed for macrostructure segmentation of a shell image into its component parts. The boundary detection technique employed was straightforward threshold detection; conventional boundary following techniques were used.

Figure 16 shows a typical scan line across one projectile in which cavitation was encountered; the density depression corresponding to the cavity is encircled. The least dense portions of the scan line (labelled 1 and 2 in Figure 16) correspond to the case-filler boundaries. The outer boundaries of the shell (labelled 3 and 4 in Figure 16) were detected by the onset of a change in slope of the scan line. These criteria were applied to each scan line beginning at the projectile base and extending to a point above the fuse well. The boundaries having been detected, the image of the filler was segmented in the previously mentioned segments from the known dimensions of the projectile. The foregoing image processing was performed on a line-by-line basis, without the necessity of storing in computer memory the entire image array.

3.5 Cavity and Crack Detection

The algorithm for defect detection was of the general class called sequential similarity detection algorithms (SSDA). This involves pre-establishing a set of prototype templates which adequately describe regions of a scene. In the present instance, the templates consisted of a set of vectors C ,

$$C = [t^1, t^2, \dots, t^k]$$

Each template t^i is a set of 16 numbers representing the image density profile along a 16-picture-element sequence of a scan line. Here the number of templates in the set C was 10 (i.e., $k = 10$).

It was assumed that a cavitation profile would be detectable as a small depression (0.02 - 0.06 density units) in a raster line scanned perpendicular to the long axis of the shell image.

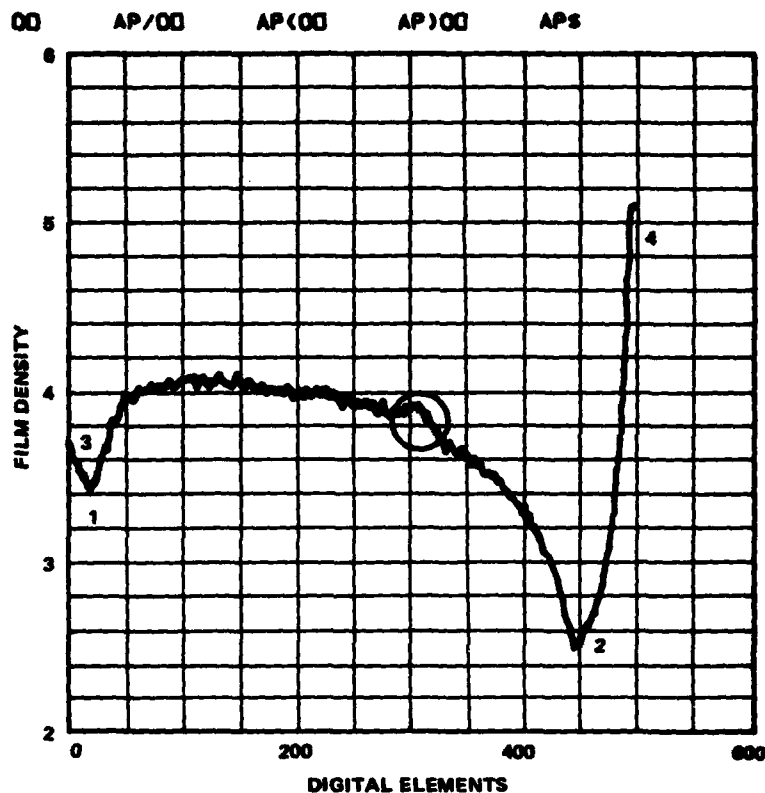


Figure 16. Representative Single Scan Across a Pipe Cavity (From Ref. 12. Reproduced by permission of Picatinny Arsenal, Dover, NJ, from earlier solicitation document QRI-109)

Cavity templates were obtained by taking 16 consecutive, parallel profiles from an image region known to contain a cavity; these 16 profiles were then averaged (in the vertical sense) to obtain a single smooth profile. Figure 17 shows two representative pipe cavity profiles obtained in this manner and subsequently used as templates for pipe cavity detection.

After obtaining the segment of a horizontal scan line corresponding to the high-explosive filler, that segment is represented by a vector of n sequential density values, n being greater than 16 (the number of elements in a template), but less than 128. The vector x is divided lengthwise into overlapping subvectors x^f , each with 16 consecutive density values (there are $n-16+1$ such subvectors, corresponding to a 16-element window moved in unit increments across x).

Each 16-element subvector is then compared with each of the 10 distinct 16-element defect templates. The degree to which the subvector matches the set C of 10 templates is measured by a "normalized error" defined by the relation

$$e(x_i^f, t_i^k) = \frac{(x_i^f - \bar{x}^f)}{\sum_{j=1}^{16} |x_j^f - \bar{x}^f|} - \frac{(t_i^k - \bar{t}^k)}{\sum_{j=1}^{16} |t_j^k - \bar{t}^k|}$$

Here \bar{x}^f is the mean of the 16 density values composing x^f , and \bar{t}^k is the mean of the 16 density values composing the template t^k . (Parallel vertical bars denote absolute value). The subscript i denotes the i -th element of

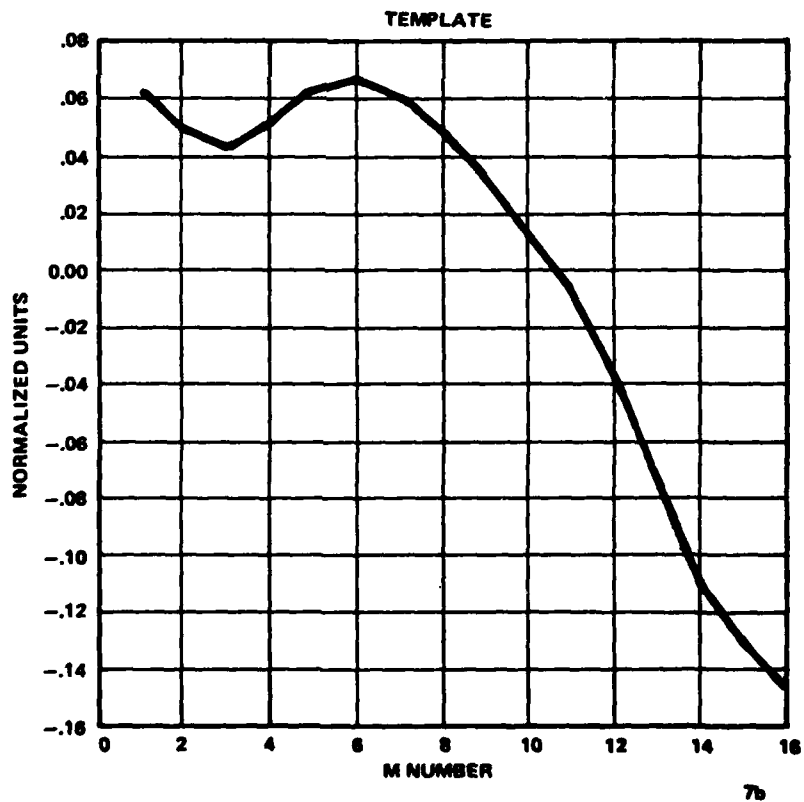
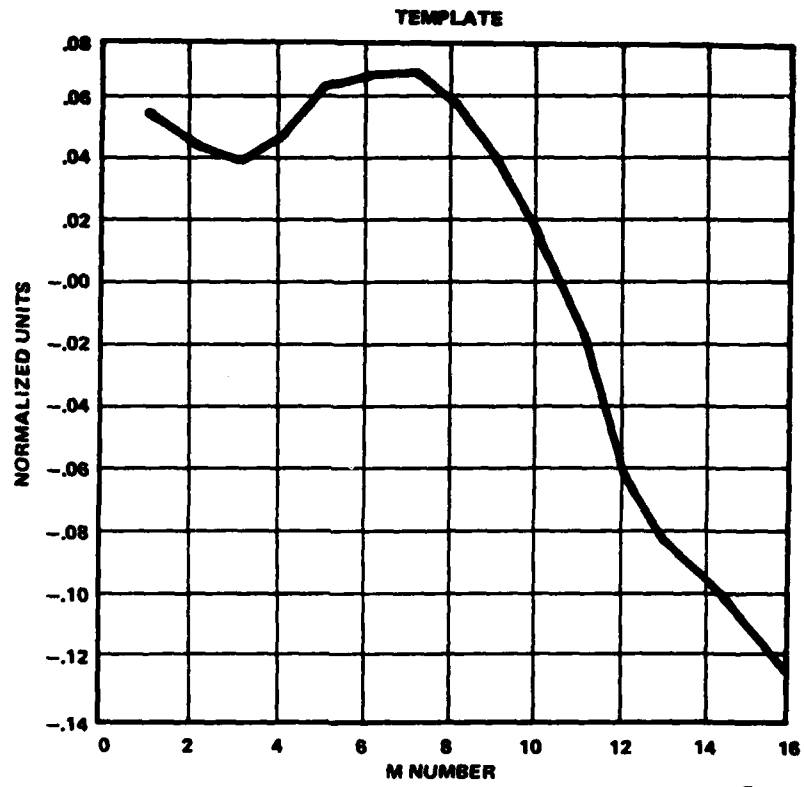


Figure 17. Two Representative Pipe Cavity Profiles Used as Templates for Pipe Cavity Detection
(From Ref. 12, Reproduced by permission of Picatinny Arsenal, Dover, NJ,
from earlier solicitation document QRI-109)

the 16-element subvector x^j ; the subscript j denotes the j -th element of the 16-element template t^k . A cumulative error function with respect to the template t^k is defined by the relation

$$E_M^k(x^j, t^k) = \sum_{i=1}^M \alpha(x_i^j, t_i^k).$$

Here M takes one of the values $M = 1, 2, \dots, 16$. Again note that for an exact match between x^j and t^k , the cumulative error remains zero for each value of M up to and including $M = 16$. For a poor match, the cumulative error grows rapidly with M .

Figure 18 shows a representative cumulative error function for a specific window x^j which does contain a cavitation, and a cumulative error function for another window which does not contain a cavity. As the normalized errors for each successive element in a window are added (i.e., as M is increased), the cumulative error for the cavity-free subvector x^j rapidly builds up; when M gets to 6, the cumulative error already exceeds the threshold value T_k arbitrarily selected for this case. On the other hand, for the x^j containing a cavity feature, the cumulative error remains below the T_k line all the way out to $M = 16$.

Thus the template t^k which most nearly matches a window x^j minimizes the slope of the E versus M graph. An integer $I^k(x^j)$ is defined to be the largest value of M such that the cumulative error $E_M^k(x^j, t^k)$ is less than the threshold value of the threshold line T_k ; one can then select a single integer $I(x^j)$ by choosing the specific template t^k which results in the largest value of M before the cumulative error $E_M^k(x^j, t^k)$ crosses the threshold function T_k . As each x^j for each raster line is examined in succession, a surface of these I maxima defining the HE filler region is formed. Regions of high relative I correspond to regions of high cavity probability. Only these local regions need be examined in subsequent measurement and classification phases.

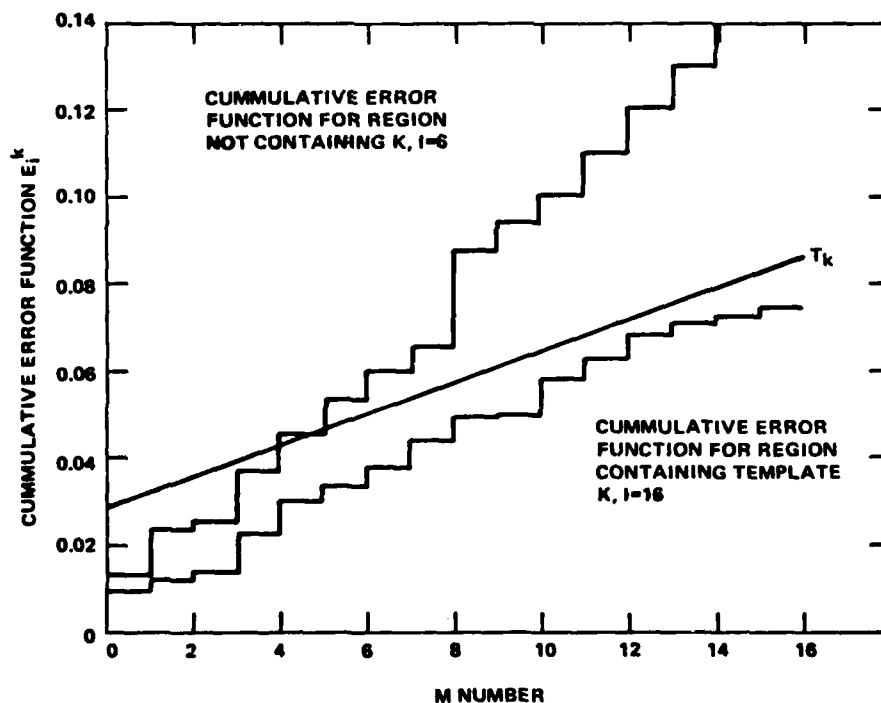


Figure 18. Cumulative Error Function and Threshold Function for Representative Template (From Ref. 12, Reproduced by permission of Picatinny Arsenal, Dover, NJ, from earlier solicitation document QRI-109)

In a representative output from the SSDA of a radiograph of four shells, 95 percent of the picture elements were eliminated before $l = 3$. This is said to represent a factor of 10 improvement in computer time over classical correlation measures using 10 templates. In this example, $l = 12$ was taken to indicate a region with high probability of containing a flaw. It is claimed that all actual cavities in these four shells were detected, along with several indications which proved to be false (the actual number of "false alarms" was not reported).

Kruger et al. note that the SSDA approach can be generalized to two dimensions if it should prove necessary for defect classification (Ref. 12). They further suggest that an intensified 500- or 1000- line vidicon may possess sensitivity and resolution adequate to replace film. They further claim that an entire four-shell scene could be real-time captured and stored in digital mass memory, and that the requisite SSDA algorithms could be implemented in either hard-wired form or in programmable microprocessors.

4.0 FILMLESS IMAGE ACQUISITION SYSTEMS

4.1 Introduction

For many applications it would be desirable to eliminate photographic film as a part of the automated radiographic process. The oldest alternative to film is the fluoroscopic screen comprising a thin layer of a finely powdered fluorescent chemical such as zinc sulfide mixed with a binder and supported by a thin sheet of cardboard or plastic. Under x-ray excitation such screens emit visible light, the brightness of which generally increases with the x-ray intensity at the screen. Originally fluoroscopic screens were viewed by eye, often by means of a mirror to minimize exposure of the eye to x-rays; it is now commonplace to employ a closed-circuit television system with the camera viewing the fluoroscopic screen and the image being remotely presented on a television screen, a video tape recorder often being used to record the image electronically.

Several alternatives to the fluoroscopic screen have been explored. These include principally the directly x-ray sensitive vidicon television camera tube; solid-state radiographic screens of the photoconductive-electroluminescent type; and scanning x-ray beam (as "flying spot") systems.

For various reasons none of these approaches has as yet found widespread industrial NDT application, but all are judged to be potential candidates for filmless image acquisition for future automated radiographic systems for at least some applications. Available information about these approaches is reviewed in the remainder of this chapter.

4.2 X-ray Sensitive Image Intensifier Tubes

Electronic image intensifying tubes, originally developed for intensifying ordinary optical images (e.g., for night viewing) have been adapted for radiographic applications. Figures 19 and 20 illustrate schematically the construction of two versions of such tubes. X-rays, having passed through a specimen, fall upon a fluorescent screen inside the vacuum envelope of the tube; the fluorescent screen is in contact with a photo-cathode which emits electrons in proportion to the intensity of light emitted by the fluorescent screen, which in turn is related to the x-ray intensity. The electrons are electrostatically accelerated and focused onto a second smaller fluorescent screen where the image reappears smaller and much brighter. The intensified image may be viewed directly or indirectly by eye, but it is now common to substitute a television camera with the image being presented on a television screen, sometimes with a television tape recorder serving as an intermediary.

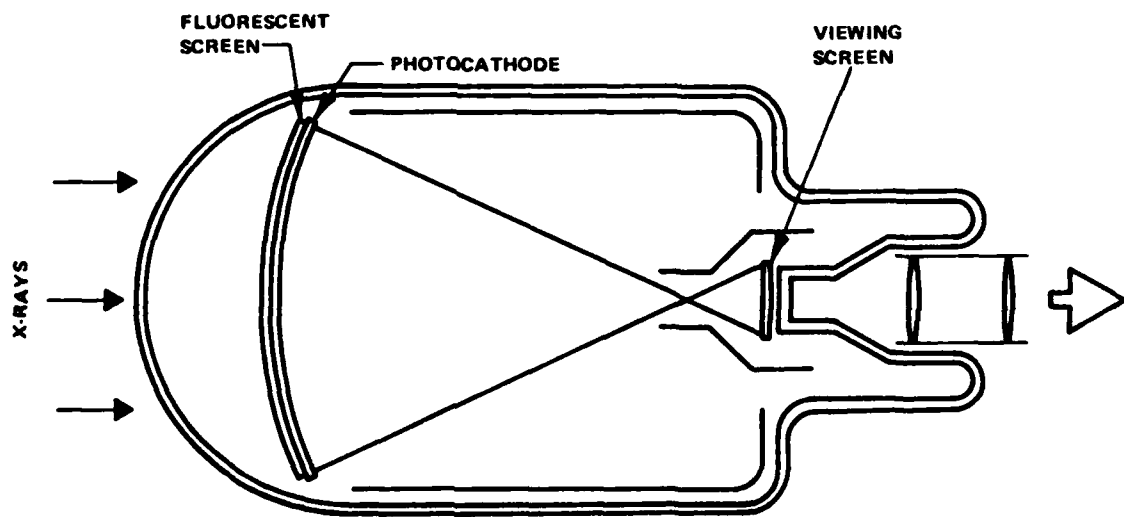


Figure 19. Schematic Diagram of a Philips Type Image Intensifier Tube (From Ref. 4, Reproduced by permission of Butterworths, London, England)

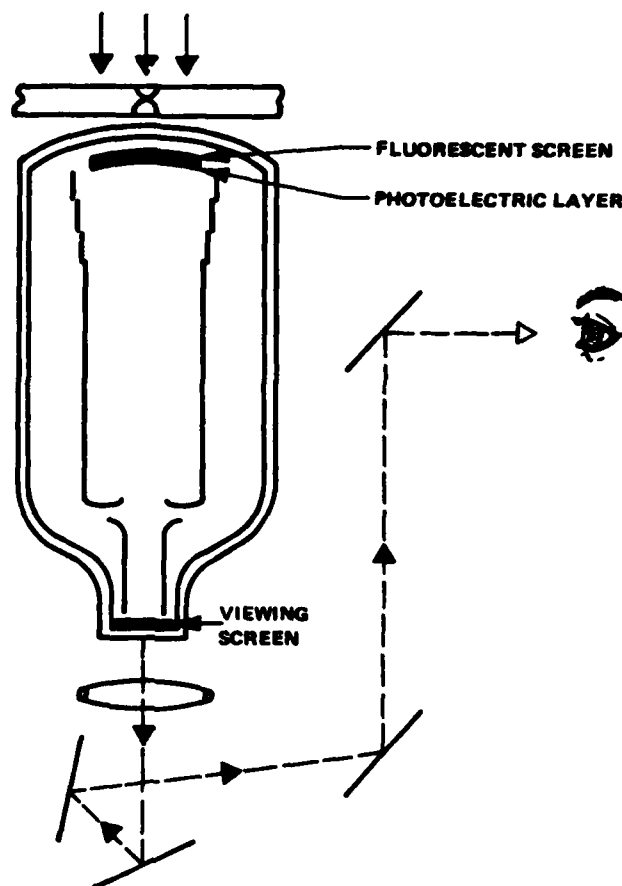


Figure 20. Schematic Diagram of a Marconi-Fluorex Image Intensifier Tube (From Ref. 4, Reproduced by permission of Butterworths, London, England)

4.3 Fluorescent Screen Plus Television Camera Tubes

4.3.1 Fluorescent Screens plus Image Orthicons

When the image produced by a conventional x-ray sensitive fluorescent screen is sufficiently bright, its image can be picked up by a sufficiently sensitive television camera tube. Vidicon type tubes have generally proved insufficiently sensitive, but orthicon type tubes have worked. An industrial system of this type (the "Lumicon") has been marketed. An evaluation of this early system was made by Criscuolo and Dyer (Ref. 13). Another version of this type of system, intended for medical applications, was produced in the United Kingdom; Figure 21 shows modulation transfer function curves for this system as given by Halmshaw (Ref. 14).

Utilizing a recently patented fluoroscopic screen (Ref. 15), a fluorographic sub-system for an automated ultrasonic fluorographic welded-pipe inspection system has been developed by U.S. Steel Corporation (Ref. 16). Light from a special "single crystal" screen is gathered by a conventional lens system and is directed onto the face of a specially designed image isocon TV camera. The image signal is amplified and available for direct viewing and storage. In the storage mode the TV signal is first enhanced by repetitive scanning onto a silicon target. Thirty-two integrations (signal averaging) provide a factor of 5 boost in signal-to-noise ratio.

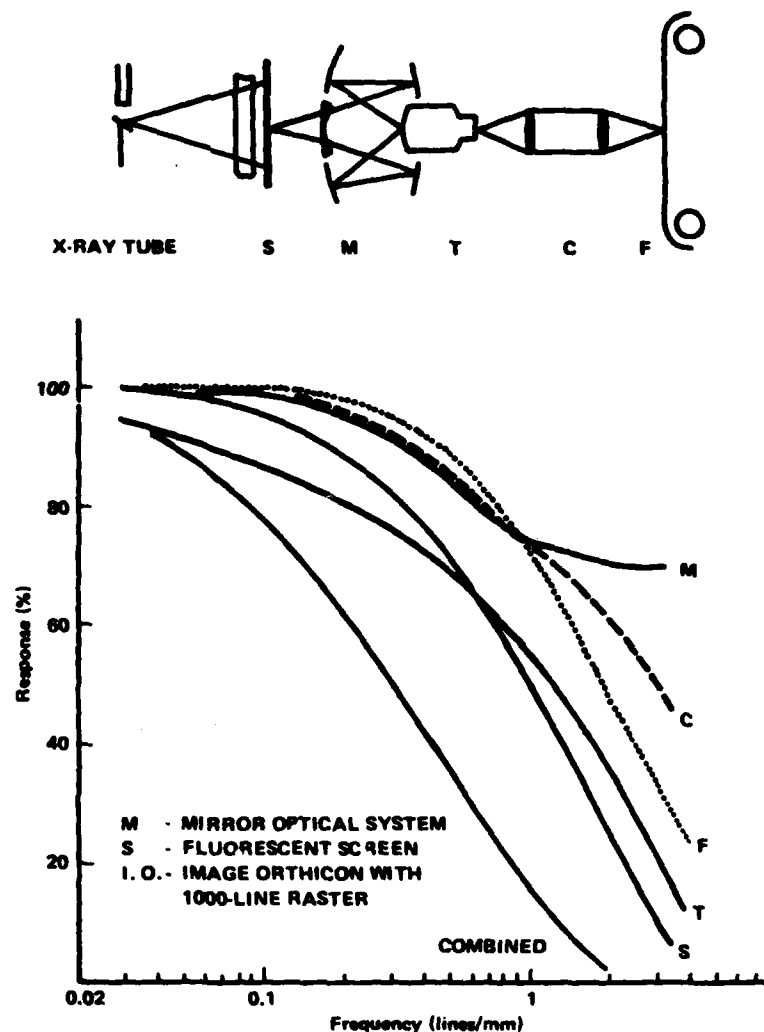


Figure 21. Modulation Transfer Function for a Fluorescent Screen/Image Orthicon Television System, Calculated from MTF data for the Components (From Ref. 14, Reproduced by permission of Academic Press, Inc. (London) Ltd.)

4.3.2 Fluorescent Screen plus Light Intensifier Tubes, plus TV Vidicons

Conventional light image intensifier tubes are of essentially the same construction as that of Figure 19 or 20 except that the primary fluorescent screen is omitted. They are thus essentially visible light image intensifiers. Tubes of this type have been used in conjunction with conventional external x-ray sensitive fluorescent screens. Typically such systems employ efficient light gathering optical systems. The "cinelex" system of this type is illustrated in Figure 22. Because of the brightness of the output image from the image intensifier tube, the simple but relatively insensitive television camera tube of the vidicon type can be used in this system. Modulation transfer function curves for the various components of this system, and for the system as a whole, (as given by Halmshaw, Ref. 14) are shown in Figure 23.

4.4 X-Ray Sensitive Television Camera Tubes

An x-ray sensitive television camera tube NDE application was conceived and proposed by Hastings (Ref. 17), and later developed by Watertown Arsenal/A. B. DuMont Labs. The General Electric Company

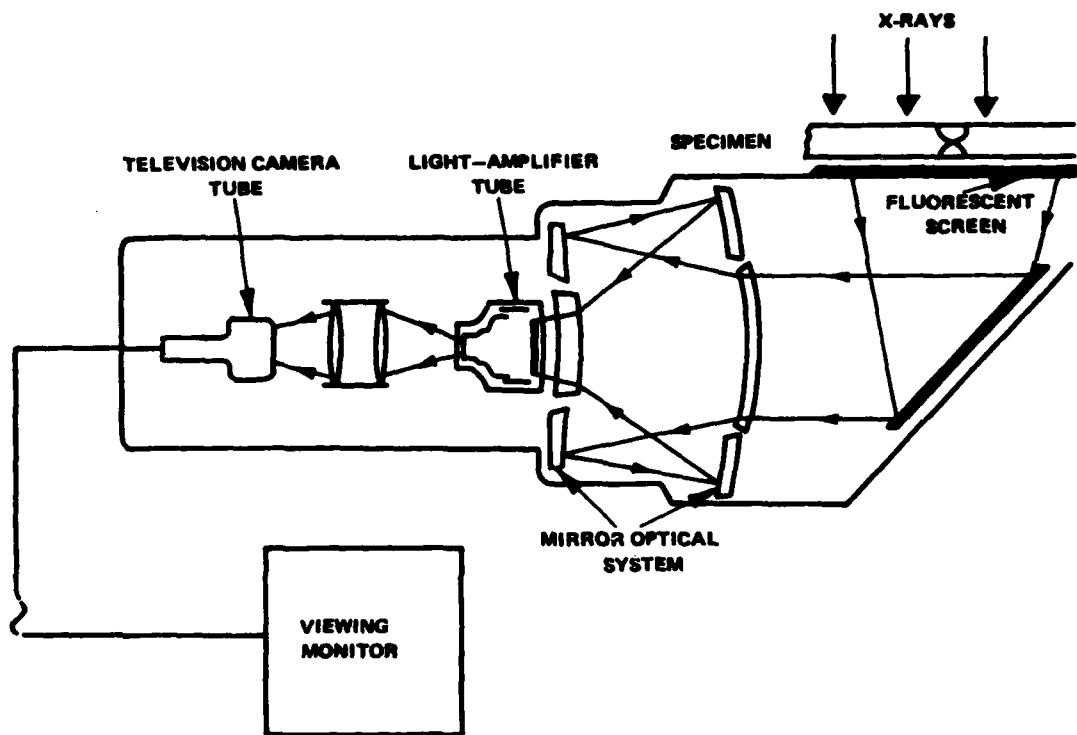


Figure 22. Schematic Diagram of Cinelix Image Intensifier Apparatus (From Ref. 4, Reproduced by permission of Butterworths, London, England)

also developed a system for the commercial market (Ref. 18). McMaster et al (Ref. 19) developed a tube, and a commercial version was marketed by Philips Electronics Instruments Division (Norelco). Figure 24 is a schematic drawing of the tube; Figure 25 is a schematic of the entire system, including a conventional cathode ray tube television image display. Numerous applications and evaluations of the commercially available system have been reported. Halmshaw (Ref. 14) summarizes this system's characteristics as follows:

- (a) A high exposure dose rate (10-1000 R/min) is required at the pick-up surface, up to 150 kev (above this energy performance degrades).
- (b) The sensitive area of the camera tube is about 1/2 in. \times 3/8 in.; hence, application is therefore limited to very small specimens, or else scanning is required.
- (c) Attainable image definition is good, permitting the 1/2-in. wide image to be displayed on 17 in. TV monitor screens.

According to Halmshaw (Ref. 14), x-ray sensitive television camera tubes up to 9 in. in diameter have been constructed, but not marketed. There appears to be no effort at present to produce larger diameter tubes, although such tubes, if they were sensitive to x-rays of energy commonly used in industry, would seem to have many applications. In particular, they would seem to offer many advantages for image acquisition for fully automated radiographic systems. A strong advantage is, of course, that the image information is immediately available as an analog electronic signal which can be pre-processed in analog form, and is also readily converted to digital form.

In medical applications where minimum exposure dose is sought, the fluoroscopic image is dim and either an electronic image intensifier is used in conjunction with the electronically simple but relatively insensitive vidicon camera tube, or the more sensitive (and electronically more complex) image orthicon camera tube is used. The introduction of the television intermediary has the advantage of permitting

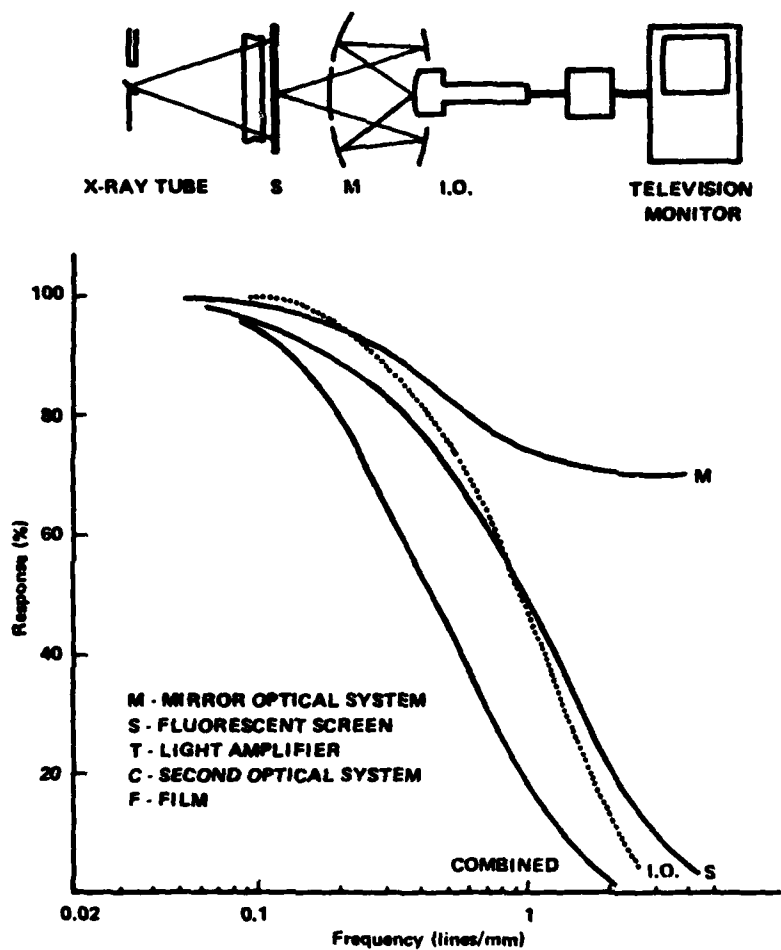


Figure 23. Modulation Transfer Function for System Comprising a Fluorescent Screen, Mirrors, Light Amplifier, and System for Film Recording (From Ref. 14, Reproduced by permission of Academic Press Inc. (London) Ltd.)

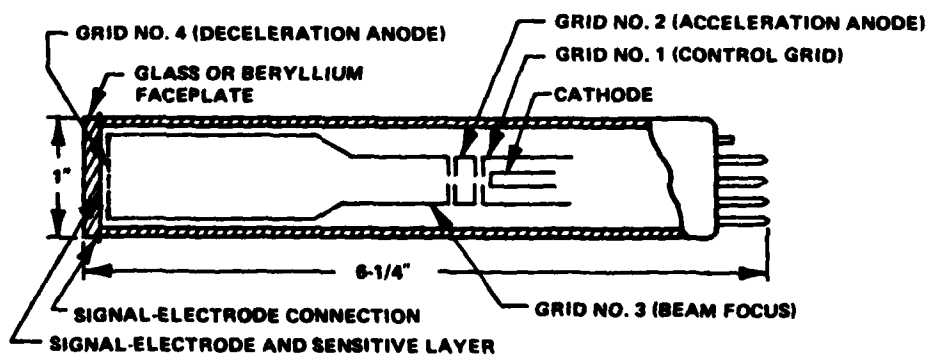


Figure 24. Diagram of X-Ray Sensitive Vidicon Tube (From Ref. 17, Reproduced by permission of the American Society for Nondestructive Testing, Inc., Columbus, OH)

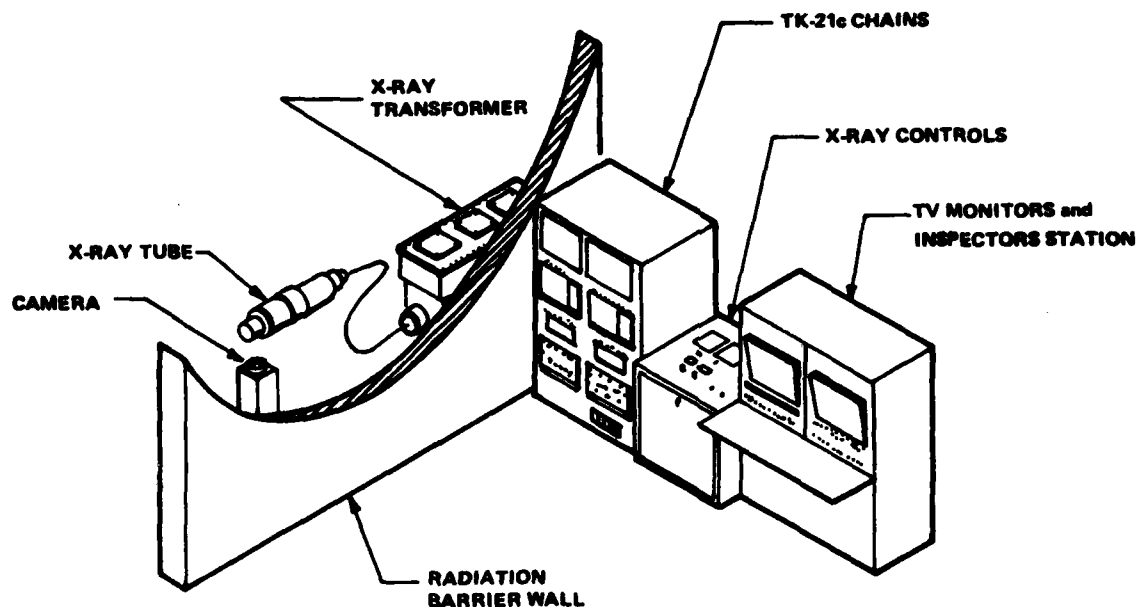


Figure 25. Skeletal of X-Ray TV System (From Ref. 17, Reproduced by permission of the American Society for Nondestructive Testing, Inc., Columbus, OH)

direct analog electronic control (within limits) of image brightness, contrast, and enlargement, and facilitates the analog-to-digital conversion of the image for computer processing. A disadvantage is the fact that the fineness of the scan raster sets a limit on the (vertical) resolution of image features; also the horizontal resolution of image features depends upon the electronic frequency bandwidth of the system. However, at the price of (achievable) complexity in electronics, the overall modulation transfer function is generally limited by the MTF of the fluoroscopic screen itself. In terms of industrial applications, the chief drawback of fluoroscopic screens is the fact that their relative brightness peaks rather sharply at effective x-ray kilovoltages in the range of 50 kvp to 200 kvp, and drops off rapidly at higher voltages.

4.5 Solid State Radiographic Screens

The solid state radiographic image converter is constructed by sandwiching a photoconductive (PC) layer and an electroluminescent (EL) layer between two electrodes. The construction is shown schematically in Figure 26. The electrode on the EL layer must be transparent to visible light; the electrode on the PC layer is opaque to visible light, and an optically opaque layer is placed between the PC and EL layers; thus, the PC layer is shielded from light, but not from x-rays. In the absence of x-rays, the electrical impedance of the PC layer is much higher than that of the EL layer; consequently, the voltage drop across the EL layer is small and the EL layer produces little or no light. When the PC layer absorbs x-rays, it becomes conductive, the voltage drop across it is small, and the voltage drop across the EL layer becomes high; thus, the EL layer emits light the intensity of which is monotonically related to the x-ray intensity. Depending upon the exact composition and processing of the PC layer, the image may have a short decay time (in which case the device is referred to as an image amplifier screen) or a long decay time, (in which case it is referred to as an image storage screen). Characteristics of a representative PC-EL amplifier screen, as reported by Szepesi (Ref. 20), are given in Table I on the following page.

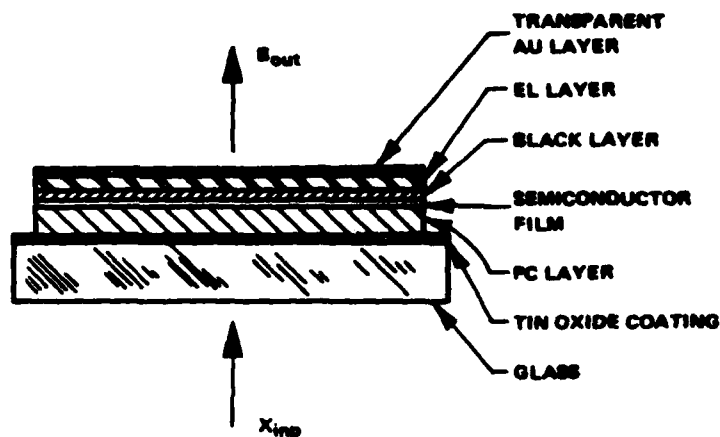


Figure 26. Schematic Diagram of Photoconductive-Electroluminescent Image Amplifier (From Ref. 20, Reproduced by permission of the Society of Photo-Optical Instrumentation Engineers, Palos Verdes Estates, CA)

Table I. Characteristics of Average Radiographic Amplifier Screen

| Characteristics | Measured Data |
|----------------------------|---|
| Max. Size | 10" x 10" |
| Resolution | 300 TV l/i |
| Driving Voltage | 100 to 250V |
| Frequency | 50 to 400 Hz |
| Max. Current | 150 μ A/in ² (60 Hz, 100V) |
| Threshold | 10 to 100 mR/min |
| Max. Brightness | 10 ⁻¹ to 10 η |
| Max. Contrast (γ) | 2 to 6 |
| Max. Gain over CB-2 | 10 to 100 |
| Response Time | 1 to 10 sec |

Typical response curves are shown in Figure 27, along with the response curves of a representative fluoroscopic screen.

A limitation of PC-EL radiographic screens is that their response to radiation above about 100 Kv is poor.

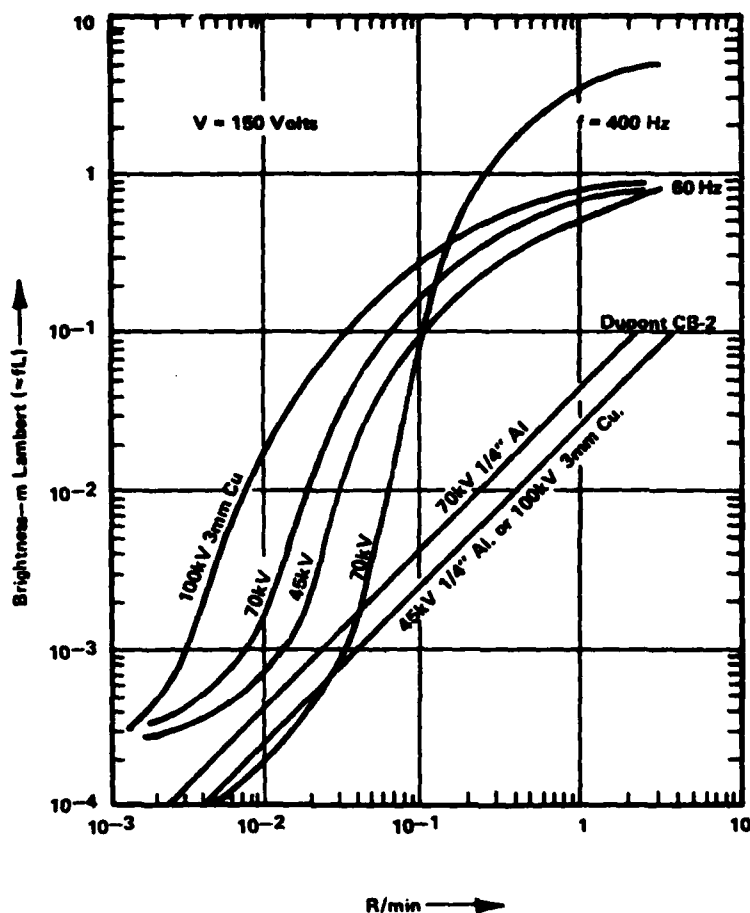


Figure 27. Transfer Characteristics of a PC-EL Radiographic Amplifier Screen (From Ref. 20, Reproduced by permission of the Society of Photo-Optical Instrumentation Engineers, Palos Verdes Estates, CA)

4.6 Flying Spot Systems

Stein and Swift (Ref. 21) describe an x-ray imaging system which employs a moving narrow x-ray beam which rapidly scans an object. The system was designed for inspection of parcels. Figure 28 shows schematically the operation of the system. The effect of the slit collimator and the rotating collimation disk is to produce a collimated beam which scans an object vertically. The object itself is translated horizontally on a mechanical conveyer belt; successive scans thus "slice" the object into a raster pattern. Changes in beam intensity are detected by a linear x-ray detector (a sodium iodide scintillation crystal coupled to a photomultiplier tube). The signal from the detector is recorded on video tape and subsequently played back on a television CRT display for visual examination. Similar systems are widely used for baggage inspection.

A variant of this system is illustrated in Figure 29. In this system, detectors are placed on the same side of the object as is the incident x-ray beam, and the backscattered radiation is detected. A prototype of this system was reported to be operational.

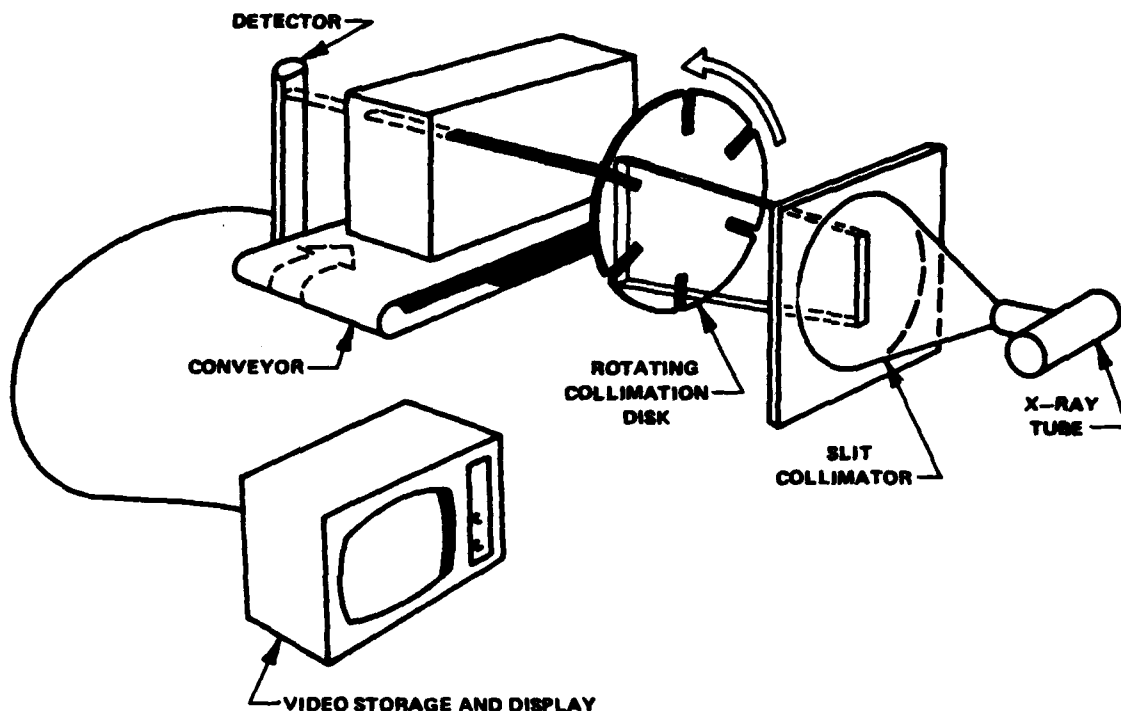


Figure 28. Schematic Diagram of a Flying Spot X-ray Imaging System for Parcel Inspection (From Ref. 21, Reproduced by permission of the American Society for Nondestructive Testing, Inc., Columbus, OH)

The effective spot size was approximately 2mm by 2mm (although the size varies during a vertical scan to compensate for variations in detector sensitivity). A single scan of a typical object required about 5 seconds. The width of the spot is reported as no more than 1/500 of the width of the image.

An important consideration with respect to this system is its low efficiency in terms of utilization of x-ray beam intensity. Of the several thousand x-ray quanta which impinge on the 2mm x 2mm spot area, only about 100 are actually detected. Hence, the average statistical fluctuation in detected beam intensity would be about 10 percent; the image thus exhibits large "quantum mottle". This can be reduced only by increasing source intensity or detector efficiency, or by slowing the scan rate.

Details of the radiographic sensitivity and resolution of this system are unavailable.

Another system utilizing similar principles is one for the evaluation of potting voids in electronic fuses (Refs. 22, 23). The system consists of a stationary penetrating collimated x-ray beam transmitted through the fuse, then through the aperture of a collimator mounted on a sodium iodide (thallium) detector unit. The detector outputs are photomultiplied and processed electronically for display in real time as relative changes in radiation transmission through the fuse volume, for various positions of the fuse. Scintillographic resolution is limited to 0.75 percent by x-ray source stability. Detection of 0.32cm voids in XM732 fuses was achieved.

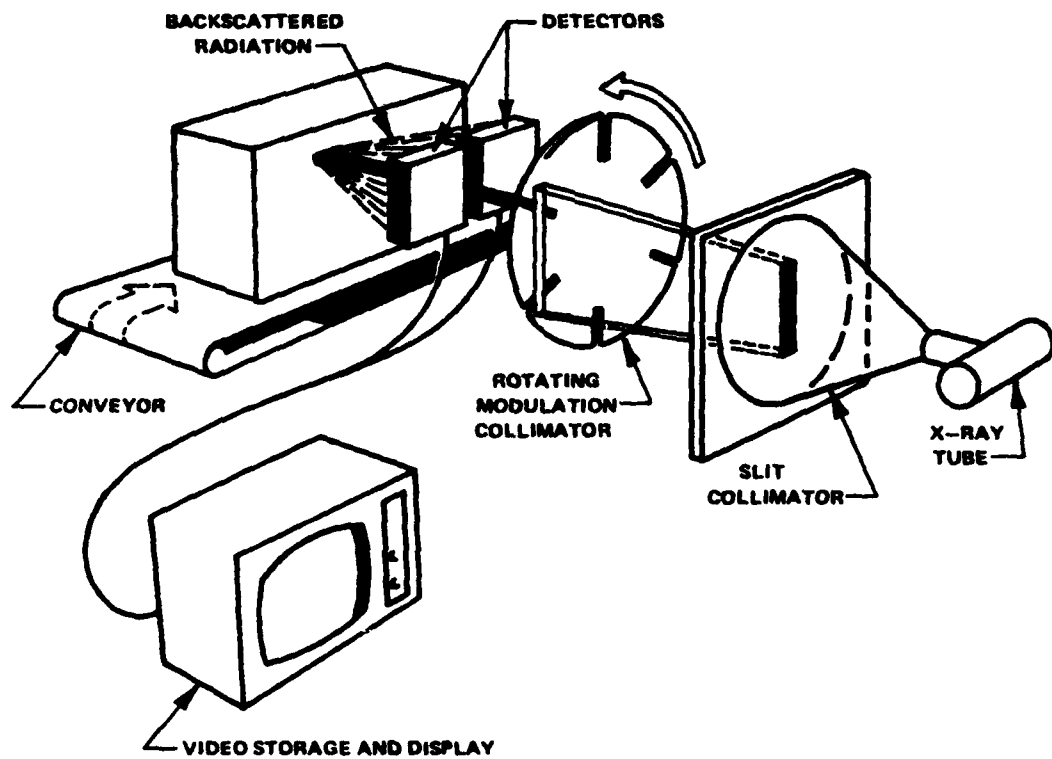


Figure 29. Schematic Diagram of a Possible Backscattered X-Ray Imaging System (From Ref. 21. Reproduced by permission of the American Society for Nondestructive Testing, Inc. Columbus, OH)

5.0 CONCLUSION

As of this writing, automated industrial radiography, in the authentic sense of the term, is not a reality. The technical route to such automated radiography, is, however, clear. The required computer technology, both hardware and software, is already available, at least for many potential applications. Relevant improvements in computer speed and architecture, size of rapid-access memory, and image analysis algorithms are outpacing other elements of the required technology. In the case where film is used as an intermediate image medium, the limiting technology is speed of image digitization. Definitive studies are needed to determine the ultimate performance achievable by straightforward extension of the present state of the art.

The most glaring deficiency in the technology for fully automated (filmless) radiography is in the image receptor. For low kilovoltage applications (up to, say, 100 Kv), presently recognized approaches may, with refinement, provide sensitivity, resolution, and aperture approaching that of film. In particular, a large aperture x-ray sensitive vidicon or alternate type of video imaging tube would appear to be attainable. Large aperture PC-EL image receptors are possible, but whether the resolution attainable can approach that of film is problematical.

For higher kilovoltage applications (~ 300 Kv and beyond), there is at present no recognized approach to an effective filmless image receptor of useful sensitivity and resolution. Here some basic conceptual advances are required. Since there is no apparent fundamental reason why such a receptor cannot be realized, the needed breakthrough probably requires only a commensurate technical effort.

Pending the emergence of a high voltage image receptor, the alternate approach of automated radiometry (radiation gauging) is a viable alternative for certain applications. The radiometric approach has been considered to be beyond the scope of this report, except for scanning systems which generate a two-dimensional grey-scale image as an output. Precisely because of present deficiencies in filmless imaging technology, radiometry is currently being studied as a means of automated inspection of artillery shells. To achieve practical inspection rates, multiple parallel radiometric channels are being considered. As of this writing, the practicability of this approach remains to be demonstrated.

REFERENCES

1. Nondestructive Evaluation, Publication NMAB-252, National Academy of Sciences, Washington, D.C., January 1969.
2. Radiography in Modern Industry, 3rd edition. Eastman Kodak Company, Rochester, N.Y., 1969.
3. R.C. McMaster, editor, Nondestructive Testing Handbook, The Ronald Press Company, New York, 1963, Vol. 1, Sections 13-27.
4. R. Halmshaw, Physics of Industrial Radiography, Heywoods, London, 1966.
5. J.W. Goodman, Introduction to Fourier Optics, San Francisco, McGraw-Hill Book Company, 1968.
6. J.E. Gray, M.P. Capp, M.D., R.R. Shannon, and F.R. Whitehead, "Modulation Transfer Function Degradation and False Resolution in Radiographic Imaging Systems," taken from Semiannual FY73 Applied Optics Research Report, Optical Sciences Center, University of Arizona, Tucson, AZ. 85721, January 1973, pp. 15-24, AD909371.
7. A. Rosenfeld and A.C. Kak, Digital Picture Processing, Academic Press, New York, 1976.
8. B.R. Hunt, D.H. Janney, and R.K. Zeigler, "Radiographic Image Enhancement by Digital Computers," Materials Evaluation, Vol. 31, No. 1, 1973, pp. 1-5.
9. A.H. Ett and E.W. Merritt, "Programmed Film Reader/Recorder," Image Information Recovery Seminar Proceedings, October 24-25, 1968, Philadelphia, PA., Society of Photo-optical Engineers, pp. 75-81.
10. A. Vary, "Investigation of an Electronic Image Enhancer for Radiographs," Materials Evaluation, Vol. 30, 1972, pp. 259-267.
11. A. Vary and K.J. Bowles, "Application of an Electronic Image Analyzer to Dimensional Measurement from Neutron Radiographs," NASA TM X-68200, National Aeronautics and Space Administration, 1973.
12. R.P. Kruger, D.H. Janney, and J.R. Breedlove, Jr., "Automated Detection of Cavities Present in the High Explosive Filler of Artillery Shells," Materials Evaluation, Vol. 34, pp. 202-206, 212 (1976).
13. E.L. Criscuolo and C.H. Dyer, "Fluoroscopic Image Intensifier Devices," Materials Evaluation, Vol. 17, pp. 344-349 (1959).
14. R. Halmshaw, Direct-View Radiological Systems (Chapter 8), in Research Techniques in Nondestructive Testing, edited by R.S. Sharpe, Academic Press, 1970, New York.
15. Roland W. Carlson, "Fluoroscopic Screen which is Optically Homogeneous," U.S. Patent 3917950, November 4, 1975.
16. E.B. Henry, Jr., J.A. Patsey, R.G. Rudolph, and D.G. Schindler, "Combined Fluorographic/Ultrasonic Inspection - A New Approach to SA-Weld Pipe Inspection, Fall 1976 ASNT Conference Paper, Houston, Texas.
17. Carlton H. Hastings, "An Evaluation of Radiography with Particular Emphasis on Detection Methods," ASTM Bulletin, pp 66-70, February 1951.
18. John Jacobs and Harold Berger, "Large-Area Photoconductive X-Ray Pickup-Tube Performance," Electrical Engineering, pp. 158-161, February 1956.

19. R.C. McMaster, M.L. Rhoten, and J.P. Mitchell, "The X-Ray Vidicon Television Image System," *Materials Evaluation*, Vol. 25, No. 3, pp. 46-52, March 1967.
20. Z. Szepesi, Improvements in Solid State Radiographic Converter Screens, in *Imaging Techniques for Testing and Inspection*, Proceedings of the Society of Photo-optical Instrumentation Engineers, Vol. 29, Los Angeles, CA., 1972.
21. Jay A. Stein and R.D. Swift, "Flying Spot X-Ray Imaging Systems," *Materials Evaluation*, Vol. 30, pp. 137-142, (1972).
22. Ruth E. Chaddick, "Radiographic Evaluation of Potting Voids in Electronic Fuses," NTIS Report AD-A033086.
23. Edward W. Burke, "Radiographic Evaluation of Potting Voids for Electronic Fuse Procurement Program: Phase II," NTIS Report AD-A035248.